Insight into large-scale LULC changes and their drivers through breakpoint characterization – An application to Senegal

Yasmine Ngadi Scarpetta, Valentine Lebourgeois, Mohamadou Dieye, Anne-Elisabeth Laques, Agnès Begue

International Journal of Applied Earth Observation and Geoinformation 132 (2024) 104066

Contents lists available at ScienceDirect

International Journal of Applied Earth Observation and Geoinformation

journal homepage: www.elsevier.com/locate/jag

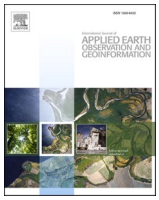

Insight into large-scale LULC changes and their drivers through breakpoint characterization – An application to Senegal

Yasmine Ngadi Scarpetta [a,b,c,*], Valentine Lebourgeois [a,b], Mohamadou Dieye [d], Anne-Elisabeth Laques [e], Agnès Begue [a,b]

[a] Cirad, UMR TETIS, Maison de la Télédétection, 500 rue Jean-François Breton, 34093 Montpellier, France
[b] UMR TETIS AgroParisTech CIRAD CNRS INRAE Univ Montpellier, F-34398 Montpellier, France
[c] UMR ESPACE-DEV, IRD, Univ Montpellier, Univ Antilles, Univ Guyane, Univ Réunion, F-34398 Montpellier, France
[d] ISRA-BAME, Route des Hydrocarbures, BP 3120 Dakar, Sénégal
[e] IRD UMR ESPACE-DEV, IRD, Univ Montpellier, Univ Antilles, Univ Guyane, Univ Réunion, Tananarivo, Madagascar

ARTICLE INFO

Keywords:
SITS
BFASTm-L2
MODIS NDVI
LSAI
LSLA
Change metric

ABSTRACT

As global land cover/ land use change (LULCC) threatens the human's well-being, accurate detection and characterization of LULCC is of paramount importance. The increasing availability of dense satellite image time series (SITS), together with the ever-improving change detection algorithms, has allowed significant progress to be made. However, much remains to be done in its characterization.

This study aims to uncover potential relationships between changes in Normalized Difference Vegetation Index (NDVI) SITS patterns and their drivers. It distinguishes itself by representing phenological changes not only as transitions between specific patterns, but also by examining the nature of these changes—whether abrupt, gradual, or seasonal. For seasonal changes, it further refines the analysis to determine their impact on the amplitude, number of seasons (NOS), or length of seasons (LOS) components. Our focus is to provide insights into the land dynamics and drivers of change in Senegal using an RGB (red, green, blue) composite change map. This map is derived from three MODIS NDVI time series change metrics detected by BFASTm-L2 within the MODIS NDVI 2000–2021 SITS: magnitude of change, direction of change, and dissimilarity of time series shape. The 250-meter resolution MODIS data served as an optimal data source for this analysis due to its high temporal resolution (near daily) and extensive coverage over 20 years.

The sensitivity of each metric to different types of change was first tested on a simulated dataset before being applied to the MODIS SITS. The RGB change map enabled visualization of different "signatures" of change, which, combined with ground information, rainfall data, NDVI time series analysis, and Google Earth imagery, helped link these signatures to various drivers of change. Climatic and anthropogenic changes, such as those induced by Large Scale Agricultural Investments (LSAI) or mining, were visually inferred from the RGB map.This approach demonstrates the usefulness of integrating the type of change, especially seasonal change, into the characterization of land change. This method has the advantage of being fast, interpretable, robust to noise and easily transferable to different regions.

1. Introduction

The Earth's land surface has been changing at an unprecedented rate, with about three-quarters of the land surface having been modified by humans within the last millennium (Winkler et al., 2021). Because such global land changes threaten the sustainability of ecosystem services and human's well-being, there is a strong requirement for monitoring land cover and land use (LULC) changes (Radwan et al., 2021). Over the past few decades, the land change community has benefited from the rapid advances in remote sensing technologies, together with the free and open data policy, cloud computing platforms, and the ever-improving change detection algorithms. Remote sensing offers significant advantages for effective land use and land cover mapping and monitoring due to its large area coverage, frequent observations at short intervals, and

* Corresponding author at: Cirad, UMR TETIS, Maison de la Télédétection, 500 rue Jean-François Breton, 34093 Montpellier, France.
E-mail addresses: yasmine.ngadi_scarpetta@cirad.fr (Y. Ngadi Scarpetta), valentine.lebourgeois@cirad.fr (V. Lebourgeois), mohamadou.dieye@isra.sn (M. Dieye), anne-elisabeth.laques@ird.fr (A.-E. Laques), agnes.begue@cirad.fr (A. Begue).

https://doi.org/10.1016/j.jag.2024.104066
Received 23 September 2023; Received in revised form 22 June 2024; Accepted 26 July 2024

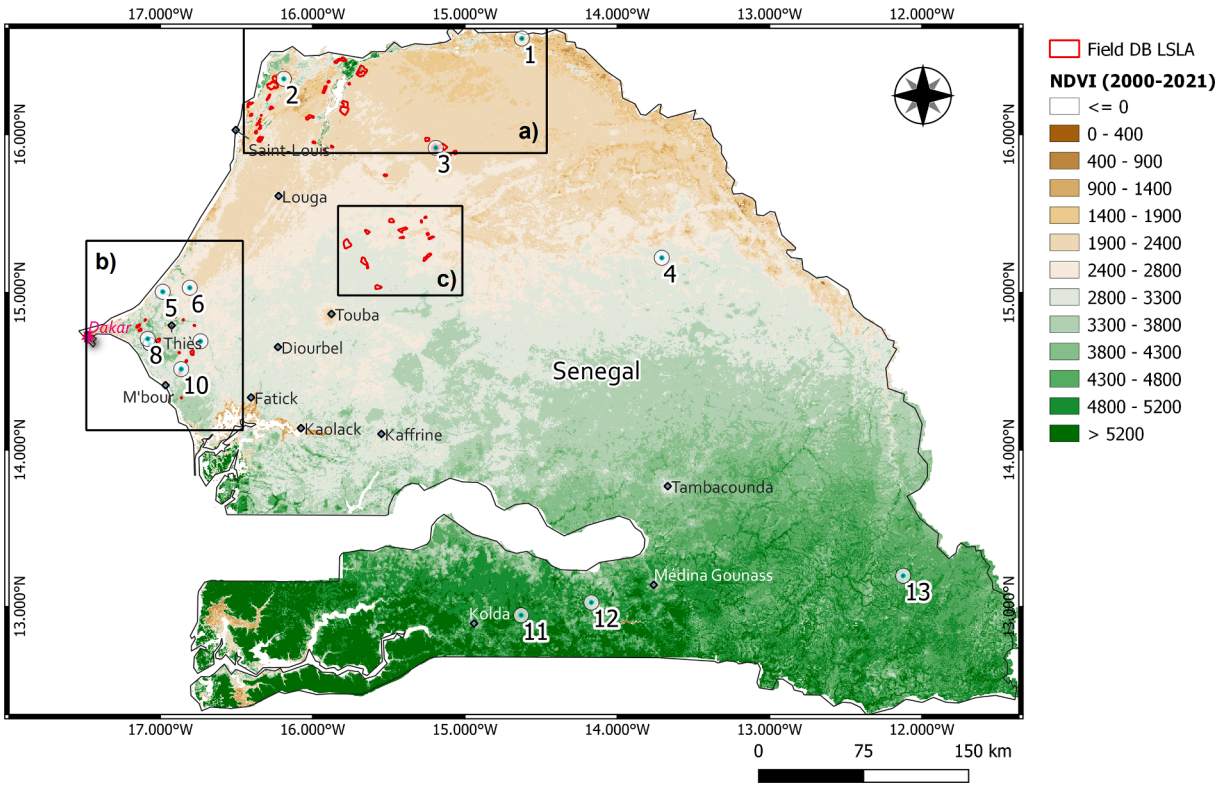

Fig. 1. Senegal's map of the MODIS NDVI 2000–2021 average. The black boxes represent the three regions of interest: a) the Senegal river (SR) (North), b) the Niayes (West), and c) Ferlo (Centre) that include most of the LSLAs (red polygons) reported in the field database (M. Dieye, personal communication, 2022. Punctual study cases used in this study are represented by points 1 to 13. (For interpretation of the references to color in this figure legend, the reader is referred to the web version of this article.)

consistent image quality. High temporal resolution remote sensing data, such as that provided by the Moderate Resolution Imaging Spectroradiometer (MODIS) sensor, allow changes to be tracked on a near-daily basis. This capability, combined with its great temporal depth, has enabled the availability of dense Satellite Image Time Series (SITS), the analysis of which has triggered a paradigm shift from bi-temporal change detection to continuous monitoring of LULC change, especially at regional and higher scales (Molinier et al., 2021; Weiss et al., 2020; Woodcock et al., 2020; Zhu et al., 2022).

Among change detection algorithms, the trend is toward those that can use all available data (and thus handle seasonal variations) in dense SITS, with supervised approaches (map classification, trajectory classification), unsupervised statistical approaches, ensemble approaches and recently, deep-learning approaches (Molinier et al., 2021). Unsupervised statistical methods, if fast enough and with few tuning parameters, are suitable for large-scale studies where the availability of labeled data at appropriate spatial and temporal resolution remains a major challenge (Woodcock et al., 2020). While they have been widely adopted by the land change community through cloud-based platforms, they still have limitations.

First, fast algorithms that do not rely on time series decomposition are more sensitive to abrupt and long-term gradual changes than to seasonal changes due to the use of harmonic regression models (Zhao et al., 2019). This can be problematic if the goal is to detect seasonal changes. In fact, specific land-use conversions, such as those driven by Large Scale Agricultural Investments (LSAIs), often include seasonal changes without abrupt changes (Ngadi Scarpetta et al., 2023). Second, algorithms that perform time series decomposition are often too computationally expensive and therefore less suitable for large-scale applications (Masiliūnas et al., 2021; Zhao et al., 2019). In addition, to the best of our knowledge, none of these statistical techniques are currently capable of both detecting and identifying the specific type of seasonal change, i.e., in amplitude, in the number of seasons (NOS) and/or in the length of season (LOS).

In an attempt to fill this gap, Ngadi Scarpetta et al. (2023) proposed BFASTm-L2, a rapid change detection approach, fine-tuned to seasonal changes. The algorithm, based on BFAST Monitor (Verbesselt et al., 2012) for breakpoint detection combined with the use of euclidean distance (hereafter referred to as L2) for breakpoint selection, demonstrated higher sensitivity to NOS changes than three state-of-the-art algorithms, allowing spatial detection of LULCC induced by LSAIs in Senegal. This and other studies (Browning et al., 2017; Hentze et al., 2017; Mardian et al., 2021; Setiawan and Yoshino, 2012) highlight the importance of accurate seasonal change detection, but also the particular link that may exist between the type and the driver of change, allowing to shift from land change detection to characterization, which remains one of the most difficult challenges in the land change community (Verburg et al., 2009; Zhu et al., 2022). Although there is no one-to-one relationship between the drivers and the types of change, some drivers are more likely to cause a particular type of change. First, climate variability often causes direct changes in amplitude through its effects on vegetation vigor and health. If important enough to change the existing vegetation cover, it impacts the overall shape of the growing cycle or Normalized Difference Vegetation Index (NDVI) cycle (Geerken, 2009), thereby affecting phenological characteristics such as the LOS or the NOS. Second, abrupt changes (often accompanied by amplitude changes) are often associated with large abiotic (fires, floods…) or anthropogenic changes. When it comes to gradual changes, land management practices inducing subtle changes, such as selective logging, reforestation, biotic changes (forest regeneration, disease…) or long trend climate change may be in cause. Finally, drivers likely to induce changes in LOS and NOS include agricultural activities (particularly agricultural intensification), that have a direct impact on the land cover type (Arvor et al., 2012; Brown et al., 2007; Hentze et al., 2017; Ngadi

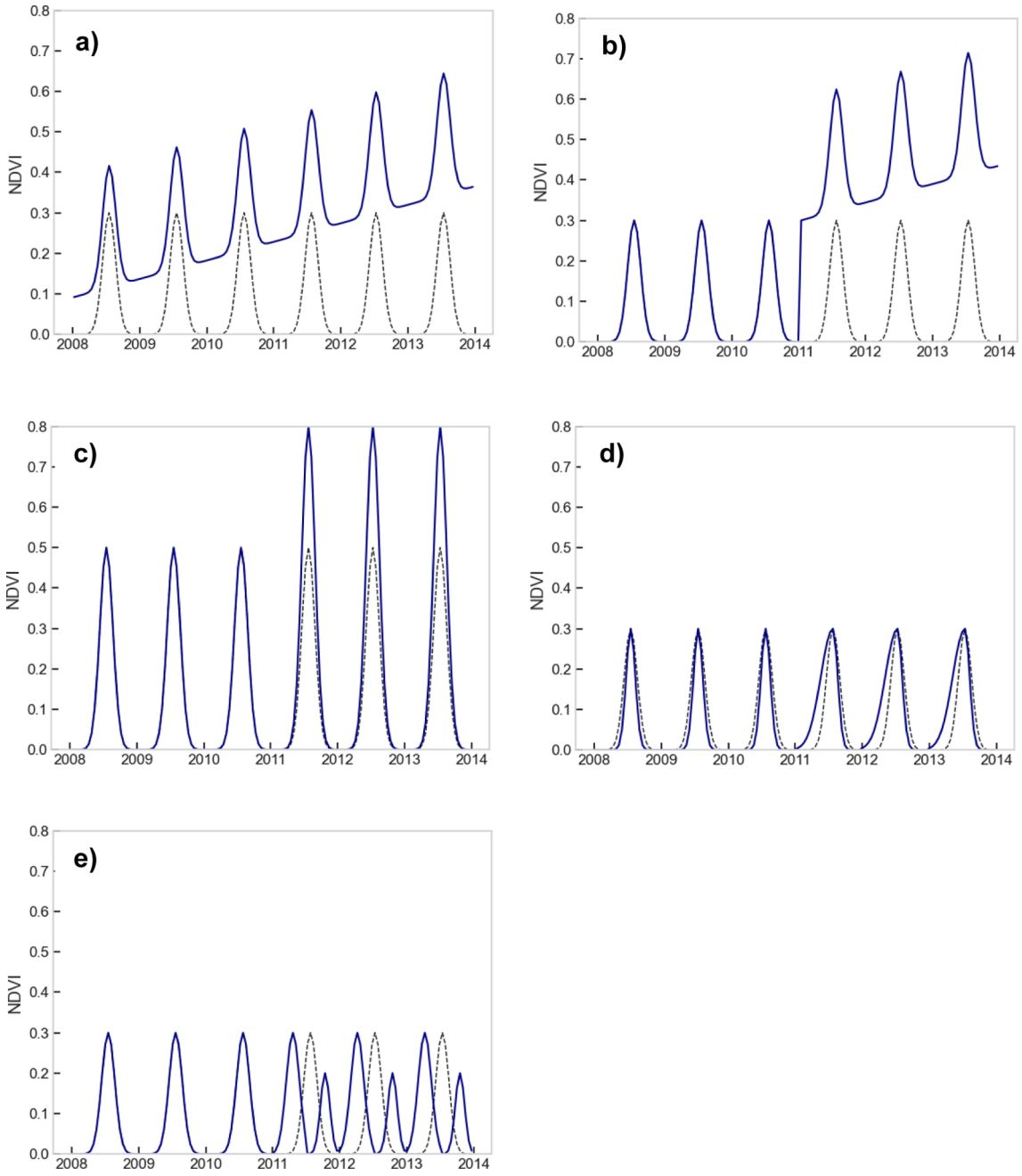

Fig. 2. Illustration of the highest-intensities changes found in (Awty-Carroll, 2019) benchmark dataset, for each change-type group: a) trend (gradual change), b) abrupt change with a gradual change, c) amplitude change, d) change in the length of season (LOS), e) change in the number of season (NOS). The no-change time series is plotted in black dash line.

Scarpetta et al., 2023).

In a recent review of the potential of remote sensing to fully characterize land change, Zhu et al. (2022) proposed a multifaceted framework consisting of five facets, including Where (i.e. the location of change), When (i.e. the date of change), What (i.e., target of change), How (i.e., the metrics of change), and Why (i.e., the drivers of change). They found that while the first three facets have been studied extensively, much work remains to be done on the last two facets.

Given the identified needs, our main objective is to contribute to the How and Why facets of land change using the BFASTm-L2 algorithm. While its sensitivity to seasonal changes was demonstrated, BFASTm-L2 also showed some sensitivity to abrupt changes and trends, hindering the analysis of land dynamics from a change type perspective. Therefore, this study aims to: i) derive a set of change metrics with varying sensitivities to the different types of change, and ii) combine these metrics into a comprehensive RGB (red,green,blue) change map to provide insight into the drivers behind the changes detected by BFASTm-L2 at the national scale. Compared to other change visualization approaches (Hird et al., 2016; Julien and Sobrino, 2021), this approach goes beyond detecting change to characterizing it (the most important change detected by BFASTm-L2 within the entire monitoring period), by looking at the specific relationships between the different types of change (particularly seasonal) and potential drivers.

In this study, special attention has been given to the detection of LSAIs. Details of the approach, data and methods are presented in the next section.

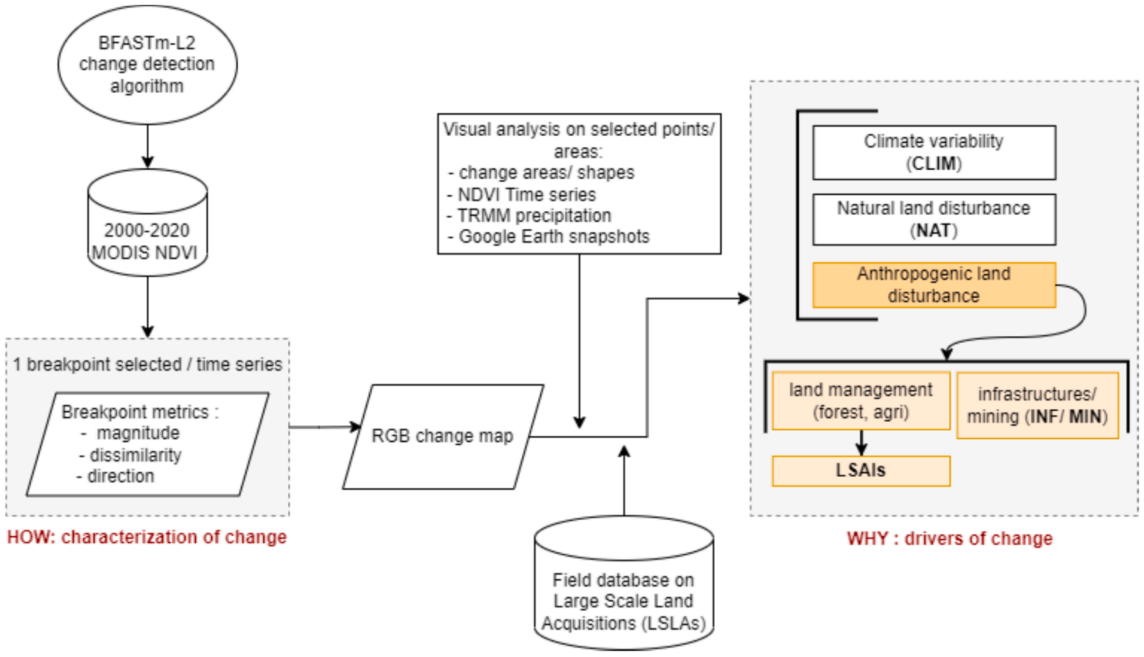

Fig. 3. Flowchart for identifying drivers of change from MODIS time series.

2. Study area and LSAI

Located in the westernmost part of the Sahel, Senegal has a strong north–south rainfall gradient resulting in a semi-arid climate in the north (200–400 mm/ year) and a tropical climate in the south (800–1200 mm/ year) (Fig. 1). Senegal has two distinct climatic seasons: a dry season from November to May and a rainy season from June to October, with the main land cover types being steppe, savanna and sub-humid dry forest (Budde et al., 2004; Sultan and Janicot, 2003; Tappan et al., 2004). It also has remarkable ecosystems, such as the productive wetlands along the Senegal River, which have supported small farmers, herders, fishermen and traders for centuries, but are increasingly threatened by dams and irrigated rice schemes (Horowitz and Salem-Murdock, 1993; Tappan et al., 2004).

The agriculture, which accounts for 15 % of the GDP, is dominated by smallholdings with farm sizes of less than 5 ha (Bourgoin et al., 2019). Large Scale Land Acquisitions (LSLAs) are however increasing in number, with 3 % of the country's arable land declared under contract by foreign investors in 2016 (Harding et al., 2016). Due to opacity, lack of geospatial information, and potential socio-environmental impacts, efforts have been made to inventory and map LSLAs (Bourgoin et al., 2019; Nolte et al., 2016). However, discrepancies and gaps remain due to the spatio-temporal dynamic nature of LSLAs and differences in methodologies. Automated and rapid approaches are needed to easily monitor the entire national territory.

Agricultural LSLAs, hereinafter refer as to Large Scale Agricultural Investments or LSAIs, are mainly concentrated over three regions, shown in Fig. 1(Bourgoin et al., 2019):

The Senegal River (hereinafter refer as to SR) region shown in box a, is an important agricultural region with a growing number of LSAIs, mainly focused on horticulture, sugarcane production and cereals, mainly rice.

The box b in the Niayes includes many LSAIs dedicated to horticulture. The vegetation consists mostly of open agricultural parkland.

The sylvopastoral area of Ferlo shown in box c, consists mainly of tree and shrub savannah, and is home to most of the LSAIs focusing on gum arabic production.

Fig. 1 also displays the locations of thirteen study cases with medium-large magnitudes of change, corresponding to different LULCCs, as interpreted using Google Earth (GE) imagery, LSAI field database, and analysis of selected NDVI time series and rainfall distributions.

3. Data

3.1. LSAI dataset

In 2019, the Senegalese Institute of Agricultural Research (ISRA) conducted a field campaign on LSLAs, with more than 700 polygons recorded in a spatial database (M. Dieye, personal communication, 2022). The database contains deal information, such as deal type (agrobusiness, mining, etc), size, year of transaction/ negotiation or implementation status. A sub-database of 76 polygons was used, which only includes: i) LSAIs established or expanded during the monitoring period (2003–2018), ii) with a minimum size of 30 ha, iii) with at least 1/3 productive area (as verified by GE imagery).

3.2. Simulated time series dataset

In this study a gap-free and noise-free subsample of the simulated time series dataset created by Awty-Carroll (2019) (https://osf.io/taf9y/) was used to analyze the sensitivity of the proposed metrics to different types of change. The subsample consisted of 3,150 simulated NDVI time series (2006–2015 at 16-day frequency resolution as MODIS), each containing a single change and belonging to one of the following change types: trend, abrupt with/without a trend change, amplitude, length of season (LOS), and number of seasons (NOS). Different intensities of change, with 50 replicates for each, were included in each group. The highest absolute intensities are (Fig. 2): 0.3 NDVI units for the amplitude changes (+60 % of the initial amplitude), a shift of season start of −45 days backward for LOS changes, + 1 season for NOS changes, 0.046 NDVI units/ year for trend changes, and + 0.3 of the NDVI baseline (+a trend of 0.046 NDVI units/year) for abrupt changes. More information (on the parameters, intensities…) can be found in Awty-Carroll et al. (2019).

3.3. MODIS NDVI data and pre-processing

The Moderate Resolution Imaging Spectroradiometer (MODIS) is a satellite sensor launched in 1999, and designed to improve our understanding of global dynamics and processes on Earth. Its global coverage, moderate spatial resolution (250 m) and high temporal resolution (1–2 days), make it ideal for detecting subtle land cover changes. Here, a set of MODIS NDVI 16-day composites at 250 m resolution (MOD13Q1, Collection 6), was acquired for Senegal over 2000–2021 and pre-processed in GE Engine. Pre-processing included the application of an optimized weighted Savitzky-Golay smoothing (Chen et al., 2004). Weights were computed according to Piou et al. (2013), which uses the reliability of the pixel (i.e., quality flag, view zenith angle) and the position of each observation in a predefined moving window (exponentially decreasing weights). A moving window length of 13 observations and a polynomial order of 3 were used.

3.4. TRMM precipitation data

Precipitation estimates for the study cases 1 (16.605°; −14.627°), 4 (15.220°; −13.708°) and 11 (12.944°; −14.631°) were obtained from the Tropical Rainfall Measuring Mission (TRMM), a satellite designed to observe rainfall in tropical and subtropical regions of the world (Kummerow et al., 1998). Specifically, the 3B43v7 product, created using TRMM-adjusted data from several sources (namely high-quality microwave data, infrared data, and rain gauges analysis), was downloaded from GE Engine. Monthly precipitation rate estimates (mm/hr monthly average) at a spatial resolution of 0.25° were converted to annual estimates (mm/year).

4. Methods

This section is divided into three sub-sections. Section 3.1 describes the global approach used in this study. Section 3.2, dedicated to the How facet of land change, presents the three change metrics derived from the MODIS NDVI SITS that characterize in different ways the change found by BFASTm-L2 between 2003 and 2018. Finally section 3.2, dedicated to the Why facet of land change, presents the RGB map obtained from the combination of the three change metrics, allowing the identification of possible drivers of change through the analysis of known study cases. Throughout this study, special emphasis was placed on the detection of LSAIs.

4.1. Approach

Flowchart of the approach is shown in Fig. 3. The first step aims to characterize BFASTm-L2 detected change on MODIS dense NDVI SITS. In addition to the magnitude of change, originally calculated by the algorithm, two change metrics were derived: a time series shape dissimilarity measure to assess the type of seasonal change, and an NDVI change ratio to assess the change's directionality. The second step aims to provide a map of the major drivers of change on a national scale by combining the change metrics into a unique RGB change map. Dominant colors were tentatively assigned to one or a few drivers of change by visual inspection using Google Earth (GE), NDVI time series analysis, precipitation distribution analysis, and the LSAI field database.

4.2. Contributing to the How facet of land change: the change metrics

4.2.1. The magnitude of change metric

The magnitude of change used in this study is the one corresponding to the largest magnitude breakpoint detected by BFASTm-L2 in each time series (Ngadi Scarpetta et al., 2023). This magnitude represents the Euclidean distance (L2) (i.e., the. square root of the sum of the squared difference) between the two 3-year time series located at each part of the breakpoint. Because this distance does not take into account the non-stationarity of the variance in the time series (Lhermitte et al., 2011), it is very sensitive to trends and amplitude changes that are commonly attributed to natural (e.g., forest regeneration) and climatic variability-induced changes, respectively. To discriminate such contributions, a time series shape similarity metric expected to be more sensitive to seasonal changes is introduced in the next section.

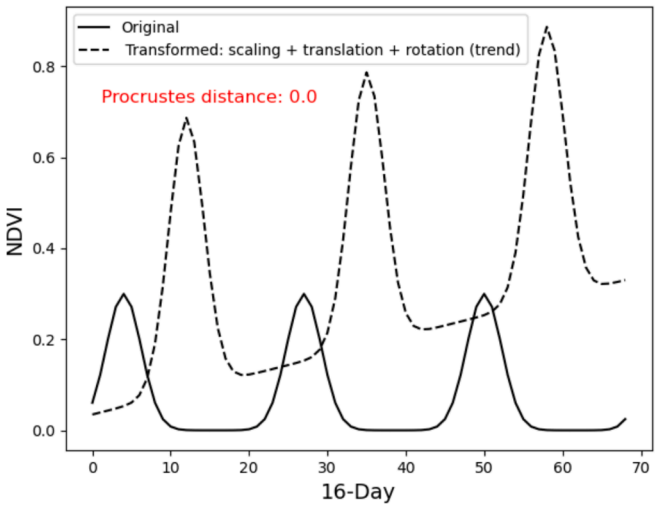

Fig. 4. Illustration of the time series (dashed) resulting from the application of scaling (x1.5 NDVI unit), translation (4 month shift) and rotation (trend of 0.1 NDVI unit/ year) transformations to the time series represented by the solid line. The computed Procrustes distance between the two time series is zero.

4.3. The time series shape dissimilarity metric

Since special attention is given to the detection of LSAIs in Senegal, that induce changes in the NDVI time series NOS and LOS components (Ngadi Scarpetta et al., 2023), we propose here the Procrustes distance (hereafter referred to as dissimilarity) as a method to refine the type of seasonal change detected. Procrustes is a measure of similarity between two shapes (or matrices), by taking into account transformations such as translation, scaling, and rotation (Gower, 1975). The goal of Procrustes analysis is to determine the minimum distance between two matrices, **X** and **Y**. This is done by minimizing the following equation:

$$d(\mathbf{X}, \mathbf{Y}) = min_{t \in T} \|\mathbf{X} - t(\mathbf{Y})\|$$

where: **X** and ***Y*** are *nxm* matrices representing the coordinates of n points in m dimensions; **T** is the ensemble of different possible combinations of scaling, translation and rotation possible, and $\|.\|$ the chosen distance norm. Values $\in [0, 1]$, with higher values indicating greater dissimilarity. Fig. 4 illustrates the time series (dashed one) resulting from the application of scaling, translation (time shift), and rotation (trend) to the original time series (solid line). Despite these significant transformations (which do not however affect the time series NOS or LOS) , the Procrustes distance between the two time series is zero.

In this study, as in our previous work on magnitude (L2) (Ngadi Scarpetta et al., 2023), we conducted a sensitivity analysis of the dissimilarity metric. This analysis was performed on both a simulated time series dataset and a selection of six real NDVI time series, including pixels with no change and pixels undergoing different types of change. For each sample, we computed the dissimilarity between two 3-year time series that were first averaged annually at each point of change. The Procrustes function from the Python spatial package SciPy was used for this calculation.

Table 1
Medians of the dissimilarities computed per type of change using the simulated dataset.

	Amplitude	LOS	NOS	Trend only	Abrupt w/ trend	No change
Dissimilarity	0.03	0.35	0.78	0.03	0.04	0.03

4.4. The change direction metric

To assess the direction of change, the ratio of the 3-year NDVI average after the change to the 3-year NDVI average before the change was calculated. An NDVI ratio below 1 indicates a "negative" direction of change, while a ratio above 1 indicates a "positive" direction of change.

As for the magnitude in our previous study, a sensitivity analysis of the NDVI ratio to different types of change was performed on the simulated time series dataset and on a selection of real NDVI time series.

4.5. Contributing to the Why facet of land change: combining the change metrics into an RGB composite map

In light of the observations made in the introduction about the relationships that may exist between specific drivers of change and the types of change observed within the time series, we propose a composite RGB map based on three change metrics having contrasted sensitivities to different types of change to help discriminate between different drivers of change: the magnitude of change (L2) in red, the NDVI ratio (indicative of the direction of change) in green, and the dissimilarity (Procrustes distance) in blue. The dominant change "signatures" (i.e. colors) observed in the RGB map were linked to specific land dynamics and drivers of change (see Table 3) based on the: i) expected relationships between some drivers and types of change (presented in the Introduction), ii) visual verification of thirteen selected study case points presenting different land use transitions, iii) constructed knowledge of LSAIs, and iv) comparison of NDVI time series and the distribution of annual average precipitation for cases that are likely to be non-anthropogenic due to their area and shape (cases 1, 4, and 11). As BFASTm-L2 breakpoint detection is based on the comparison of two 3-year time series subsamples, only potential drivers with short-term effects were considered and grouped into four broad classes: CLIM (for changes induced by climate variability), NAT (for biotic natural changes), MIN/INF (for mining/ infrastructure), and LSAI (for intensive agricultural activities), the latter being our main focus in this study.

5. Results and discussion

5.1. Sensitivity assessment of the dissimilarity and NDVI ratio metrics

The sensitivity of the dissimilarity and NDVI ratio metrics is here assessed using two different datasets.

5.1.1. On the simulated dataset

5.1.1.1. The dissimilarity metric. Table 1 shows the dissimilarity medians computed for each type of change in the simulated dataset. Null values are observed for "vertical" changes, represented by changes in amplitude, trend, and abrupt changes (with/without trend changes). In contrast, it is very sensitive to NOS changes (median = 0.78) and to a lesser extent to LOS changes (median = 0.35).

5.1.1.2. The NDVI ratio metric. Fig. 5 shows the distribution of the NDVI ratios for each type of change in the simulated dataset. This metric shows particular sensitivity to abrupt changes (max. = 6.03), and to a lesser extent to LOS changes (max. = 1.85). Less sensitivity is shown for amplitude and gradual changes (max. of 1.62 and 1.59 respectively). The lowest value is reached for NOS changes (1.47).

5.1.2. On real NDVI time series with different land use transitions

In this section, the MODIS NDVI time series of six pixel-study cases are presented. Four of them include LULC transitions from/to (Fig. 6.a-d): natural vegetation other than estuaries/wetlands (NAT), estuaries (EST), small-scale agriculture (SA), large-scale agricultural investment (LSAI), mining (MIN) and infrastructures (INF) (roads or airports). The computed dissimilarities and NDVI ratios are given.

Fig. 6 demonstrates that real data can be complex, with various types of changes occurring simultaneously. For example, two study cases with the same land use transition (NAT-LSAI) show different combinations of change types. While case a. shows a combination of amplitude (~ +75 %) and NOS changes, case c. shows a combination of amplitude, LOS and abrupt change. Transition SA-MINE study case b) shows a combination of all types of changes. Study cases without land conversions, i.e. cases e. and f. (NAT and EST), show mainly amplitude changes.

In this dataset the highest and lowest NDVI ratios were obtained for NAT-LSAI (case c: 2.3) and SA-MINE (case b: 0.5) transitions, due to large abrupt (~-0.1 NDVI units) and amplitude (+75 %) changes, respectively. At the opposite, the NDVI ratios close to 1 of the two cases without land conversions (case e:0.8; case f: 0.9) indicate the absence of significant land changes.

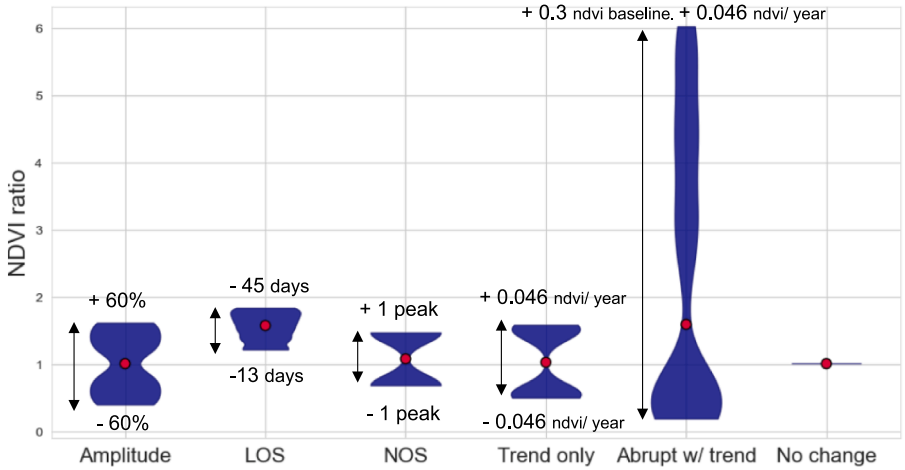

Fig. 5. Violin plots of the NDVI ratio for each type of change in the simulated dataset. Group's medians are represented by red dots. (For interpretation of the references to color in this figure legend, the reader is referred to the web version of this article.)

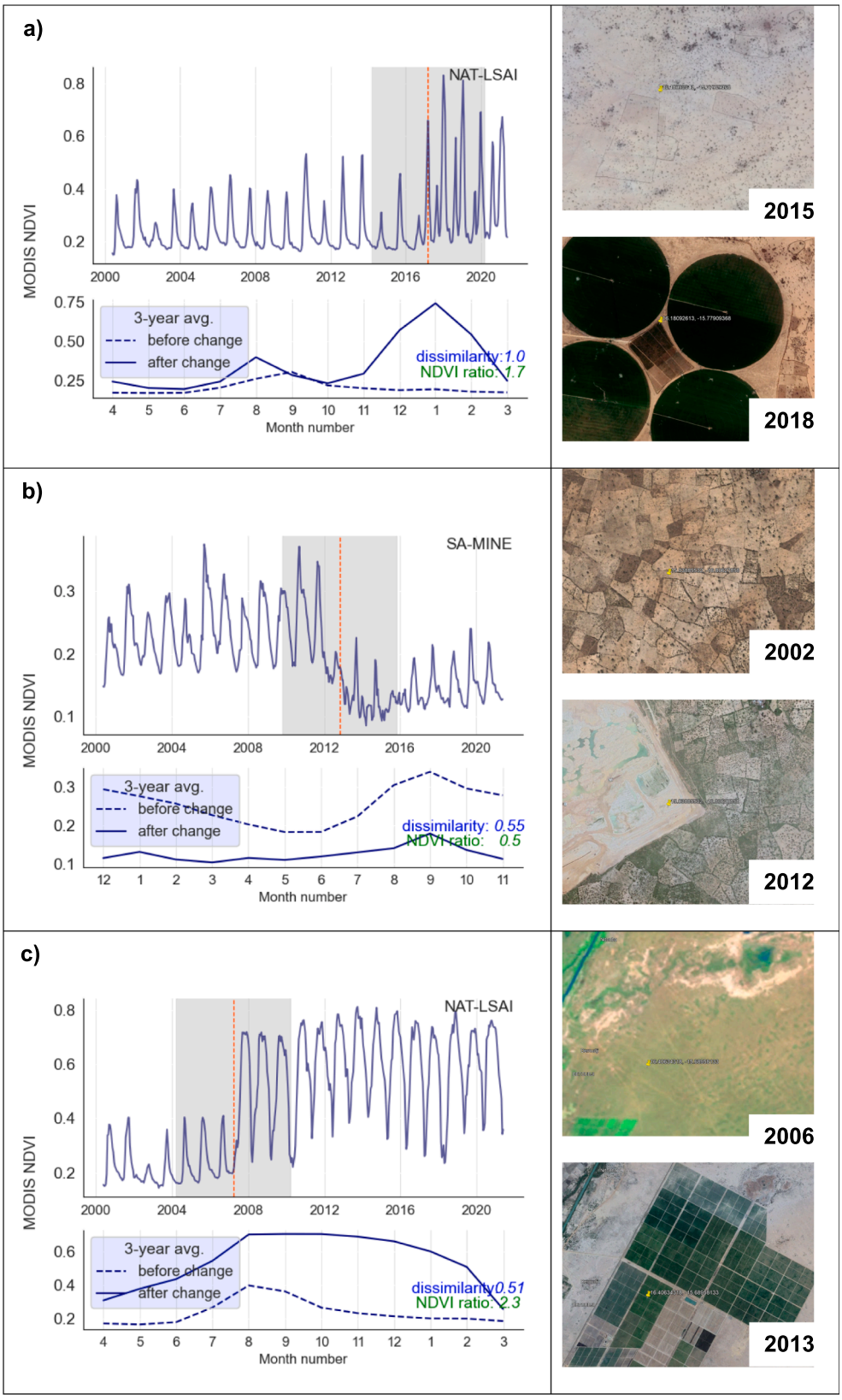

Fig. 6. Selected pixel-study cases. Each subplot's upper part shows the smoothed MODIS NDVI time series, with the breakpoint detected by BFASTm-L2 (red dashed line), and the 3-year time period before and after the breakpoint (grey zone). The bottom part shows the 3-year monthly average (before/ after the breakpoint) and the computed change metric values. Land transitions (illustrated by the GE snapshots before and after the detected breakpoint) and coordinates [latitude, longitude] are: a) NAT-LSAI [16.181°, −15.779°]; b) SA-MINE [15.039°, −16.806°]; c) NAT-LSAI [16.406°, −15.689°]; d) NAT-INF [14.708°, −17.090°]; e) NAT [16.278°, −15.312°]; f) EST [12.838°, −16.384°]. (For interpretation of the references to color in this figure legend, the reader is referred to the web version of this article.)

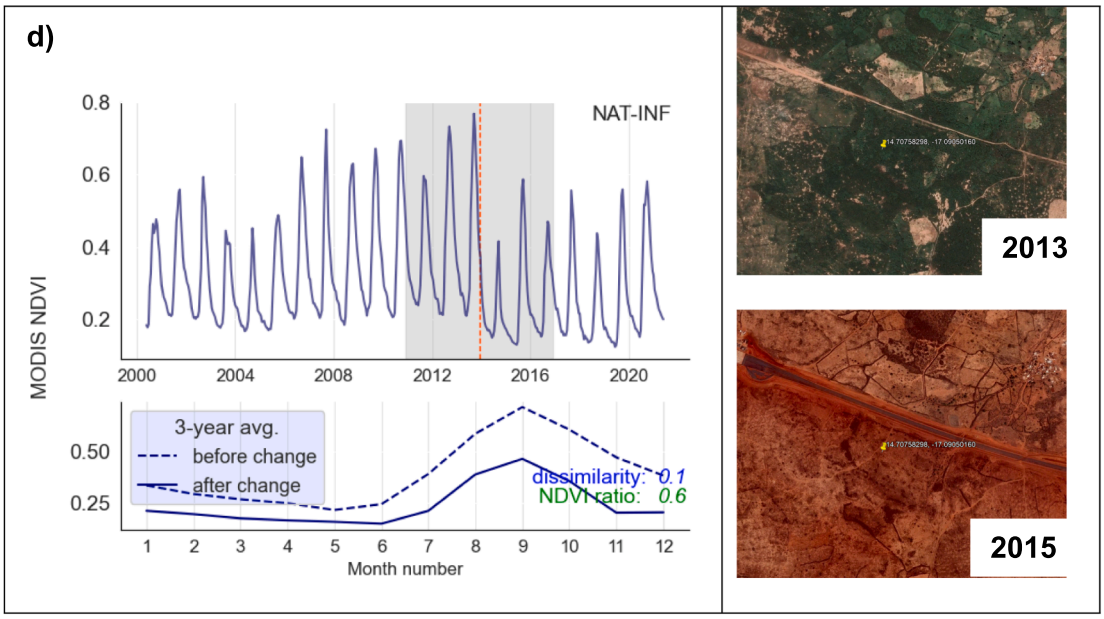

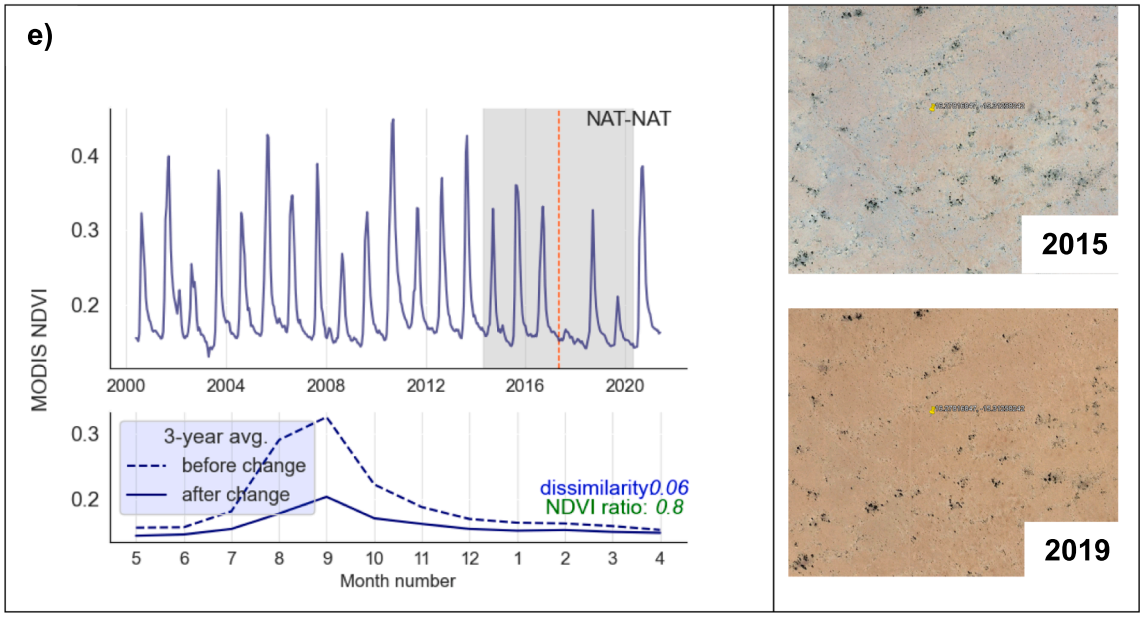

Fig. 6. (*continued*).

In terms of dissimilarity, values greater than 0.5 were observed for large-scale land use conversions, such as conversion to LSAI (case a: 1; case c: 0.51) or mining (case b: 0.55). Cases without LULCC (e.g. climate-induced changes: case e), or those covering a smaller area (e.g. infrastructure construction: case d), have lower dissimilarity values (0.06 and 0.1). An exception is the estuary study where a high dissimilarity is observed (case f: 0.61) due to the water level fluctuations.

The results are summarized in Table 2. Results related to the magnitude sensitivity were taken from a previous study (Ngadi Scarpetta et al., 2023).

Fig. 7 shows the different change metrics maps at the national scale: magnitude of change (Fig. 7.a), time series shape dissimilarity (Fig. 7.b), and NDVI ratio (Fig. 7.c). To facilitate readability, close-in views of these maps for the three regions (SR, Niayes and Ferlo) are given in Appendices B to D. As a reminder, the changes are those detected by BFASTm-L2 in the full MODIS NDVI time series between 2003 and 2018 (the monitoring period). Several observations can be made from these maps.

The first is that a breakpoint is almost always found on long and dense SITS (see Appendix A for the date of change map).

Second, the magnitude of change map (Fig. 7.a) highlights significant areas of change throughout the monitoring period. Large-scale changes (big yellow patches) are primarily concentrated in the eastern north and central pastoral regions, and the forested areas in Casamance, which are located around point 4 and point 11 respectively. The changes

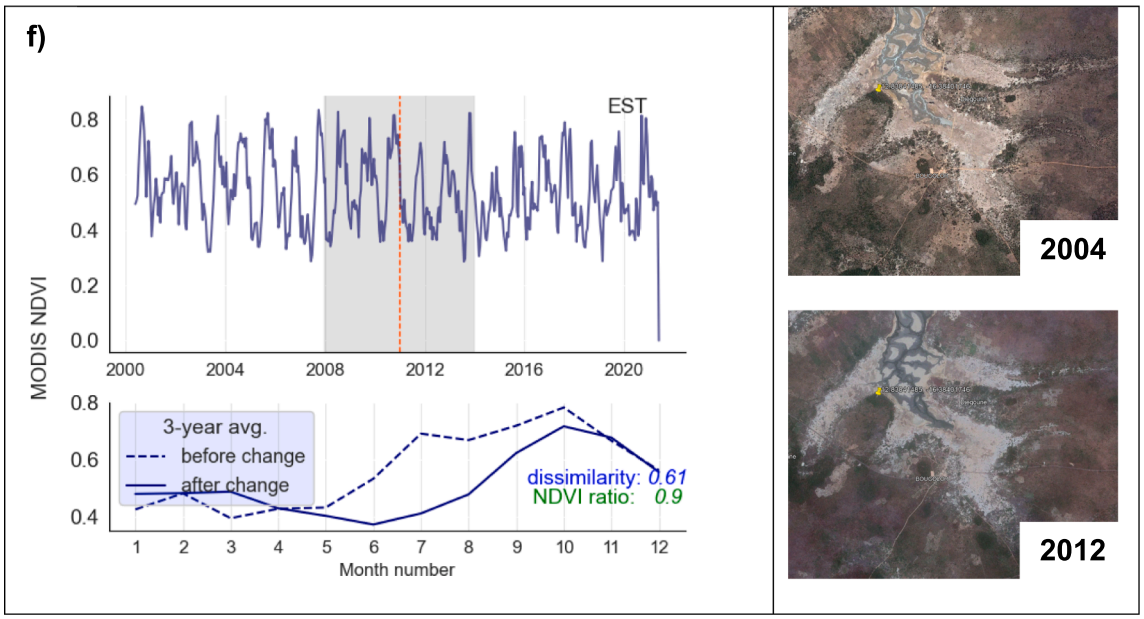

Fig. 6. (*continued*).

Table 2
Sensitivity of the change metrics to different types of change. Sensitivity classes are: low: +, medium: ++, high: +++, None: −. Change type thumbnails are for illustration only, as changes can be positive/ negative, from one direction to the other.

Change metric	Change type	Magnitude	Dissimilarity	NDVI ratio
Trend		++	−	++
Abrupt		+++	−	+++
Amplitude		++	−	++
NOS		+++	+++	+
LOS		+	++	++

occurred almost simultaneously in each region (Appendix A), indicating a common cause of change per region. At a smaller scale, it appears that the highest magnitudes in the SR (Appendix B.c) are linked with agricultural activities or wetlands, which sharply contrast with the remaining arid environment. In the Niayes (Appendix C.c), the LSAIs are well highlighted with large magnitudes of change. Additional highlighted structures include linear structures (points 7–8) that correspond to infrastructure constructions, compact patches (point 6) that correspond to mines, and more diffuse patterns over greener areas (Appendix C.a). In the Ferlo (Appendix D.c), random patterns of high magnitudes and different dates of change appear. Here, the LSAIs dedicated exclusively to the production of gum arabic do not induce visible changes.

Third, most of the previously observed magnitude hotspots disappear in the dissimilarity map (Fig. 7.b). In this map, high values are particularly observed in the SR valley, near water bodies and in the estuary regions in the south, indicating high seasonal variations. Elsewhere, the values are low, but with minor local variations. In the Niayes (Appendix C.d), the LSAIs are particularly highlighted by the dissimilarity metric. In the SR region, the LSAIs also show high dissimilarities, although they are not clearly distinguished from the surroundings characterized by the presence of wetlands. Conversely, the Ferlo region (Appendix D.d) exhibits very low dissimilarity values.

Finally, the NDVI ratio map enables evaluation of change direction ("negative" for values between 0–1, and "positive" for values > 1) and demonstrates overall similar patterns to the magnitude of change map. Very high (around 1.3) or very low (below 0.8) NDVI ratios are associated with high magnitudes of change. The most significant changes in NDVI occur in the eastern pastoral region, with a combination of high and low values (Appendix D.e). Some patterns are also observed in Casamance (southwest region), but with fewer extremes, except for the forested region near point 11 that displays high NDVI ratios. At a smaller scale, the LSAIs in the SR region are generally well represented by compacted positive change patches (point 2 and polygons in Appendix B.e), with the exception of LSAIs established prior to 2003 (Appendix B.f). In this region, the wetlands have moderate positive or significant negative NDVI ratios, suggesting that these ecosystems have mostly dried out (all causes confounded) during the monitoring period. In the Niayes (Appendix C.f), the linear structures observed in the magnitude of change map and attributed to infrastructure are well highlighted by negative values (points 7–8 of Fig. 8), as well as the mines (Fig. 9: Zoomins of study cases 1 to 13. LSAIs: 2, 3, 9, 10,12. Not in database LSAIs:

Table 3
Association table between the RGB map colours (first column) and the potential drivers of change (2nd column, see 2.4.2). Change signatures are composed of, in red: the magnitude of change, in green: the NDVI ratio and in blue: the dissimilarity metric.

Band			Possible driver of change
R: Magnitude	G: NDVI ratio	B: Dissimilarity	
-	↓ = +	+	CLIM
-	↓ = +	-	NAT, CLIM
+	+	-	NAT, LSAI
+	+	+	LSAI
+	=	+	LSAI, CLIM
+	-	-	MIN/INFR, CLIM, (LSAIs in tropical ecoregions)
+	-	+	MIN/INFR

points 5, 10. Mines: points 6 and 13. Infrastructures: points 7 (airport) and 8 (road). Forest: point 11. Wetland: point 1. Other natural vegetation: point 4..6). In this region, the LSAIs do not have overall high positive NDVI ratios, indicating less abrupt changes than in the north. The highest positive values observed here are in the form of diffuse patterns, associated with greening areas.

As observed, each map provides useful information on its own, but it is necessary to consider all three maps together for a full understanding of the changes. To this end, in the next section we propose an RGB composite map constructed to highlight anthropogenic changes.

5.2. Gaining insight into the Why facet of land change: The RGB composite map

Fig. 8 shows the national-scale RGB composite map, constructed from the BFASTm-L2 magnitude of change (red band), the NDVI ratio (green band), and the dissimilarity metric (blue band), as well as the 2000–2019 MODIS NDVI and TRMM annual precipitation distribution for 3 pixels located in large natural areas (forest: point 11, wetland: point 1, other natural vegetation: point 4). This figure is followed by close-in views over the 13 study cases (Fig. 9: Zoom-ins of study cases 1 to 13. LSAIs: 2, 3, 9, 10,12. Not in database LSAIs: points 5, 10. Mines: points 6 and 13. Infrastructures: points 7 (airport) and 8 (road). Forest: point 11. Wetland: point 1. Other natural vegetation: point 4.), to help interpret the observed signatures in terms of drivers of change.

The dominant colour observed is green, followed by yellow and orange, indicating changes with low dissimilarities. Green indicates small magnitude changes, along with varying NDVI ratio values that range from 0.73 to 1.33. Orange and yellow pixels indicate high magnitudes of change with either a decrease in NDVI average (orange pixels) or an increase in NDVI average (yellow pixels). Based on their size and irregular shape, as well as their similar dates of change (see Appendix A), it is likely that these large orange and yellow patches are caused by natural or climatic drivers of change. To confirm this hypothesis, we visually analyzed the NDVI time series and precipitation distributions from points 4 and 11 in Fig. 8. The change detected at point 4 (red dashed line in 2012) correlates with a decrease in both NDVI amplitude and precipitation, supporting the hypothesis of a climate-driven change. In fact, a drought episode that caused a major humanitarian crisis in the Sahel was reported in 2012 (United Nations Office for the Coordination of Humanitarian Affairs. Sahel Crisis:, 2023). The NDVI time series at point 11 shows a sharp increase in its baseline in 2003 (detected date of change), corresponding to an increase in pluviometry. This is consistent with positive anomalies observed in the region during the same period (Solly et al., 2020). The absence of significant seasonality changes, other than erratic amplitude changes, supports the assumption of non-anthropogenic change.

Looking closely at Fig. 9 and the sub-regional areas in Appendices B, C, additional shades of pink and blue appear that are associated with changes of greater dissimilarity values (along with varying magnitudes). The blue shades are primarily observed in the northern and southern coastal ecosystems (see Appendix B.f). These areas show small magnitudes of change and no significant NDVI changes over a 3-year period. In the arid north, areas of light pink are associated with higher magnitudes of change (Fig. 9.1), suggesting a higher degree of instability compared to estuaries in the south.

In addition to coastal ecosystems, other land dynamics are shown in light pink. This is the case for all LSAIs in the Niayes and several of those in the SR (zooms 2, 5, 7–8, 9, 10 of Fig. 9 and Appendices B.f and C.f). However, those dedicated to gum arabic production in the Ferlo do not follow the same trend (in yellow, see Appendix D and Fig. 9.3). In the SR, many of the LSAIs established before 2003 (start of the monitoring period) are colored in light pink, while the most recent ones appear in white, indicating very high NDVI ratios (zoom 2 of Fig. 9). In the southern Casamance, the LSAI plots shown Fig. 9.12 are light pink, except for the most recent plot in orange, indicating very low NDVI ratios, possibly due to vegetation removal associated with plot preparation.

As noted above, the orange color indicates changes with low dissimilarity values. It is therefore surprising that the vegetation cover's removal does not lead to higher dissimilarities. This is also the case for most changes induced by infrastructure (roads Fig. 9.8) and some mines (Fig. 9.9), which are also orange. Larger mines (Fig. 9.6, 9.13) or infrastructure (airport in Fig. 9.7) tend however to appear in dark pink, indicating higher dissimilarities.

The observations are summarized in Table 3. In this table, the

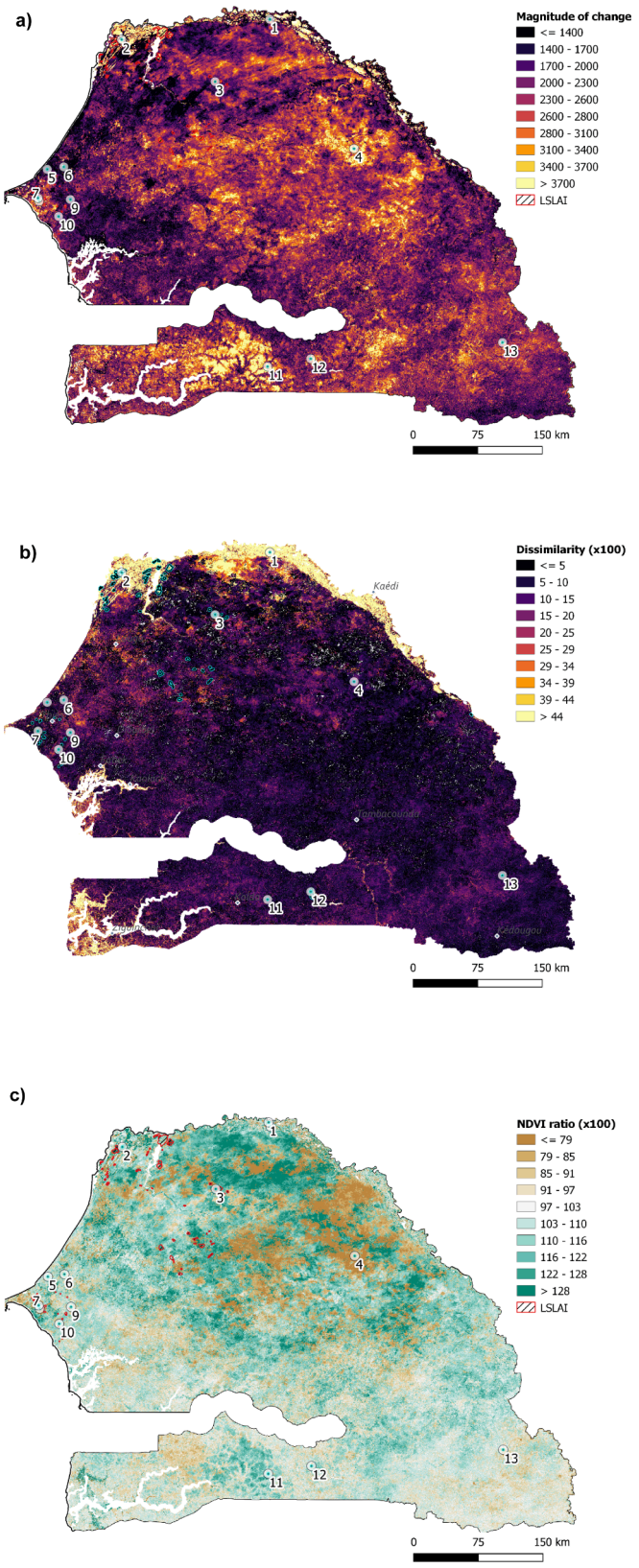

Fig. 7.. National maps of the different change metrics: a) the magnitude, b) the dissimilarity, c) the NDVI ratio.

dominant colors observed are linked to the 3-band intensities (1st column), and to some potential drivers of change (2nd column).

6. Discussion

This study aligns with recent efforts to produce improved change maps that go beyond simply identifying the timing and magnitude of change, (Rodríguez Paulino et al., 2024; Schroeder et al., 2017), with some of these efforts also addressing the characterization of detected change within spectral index time series (Chen et al., 2023; Kennedy et al., 2015; Zhang et al., 2022). However, unlike most studies that are supervised and focus on disturbances within specific ecosystems, primarily forests, this research breaks free from ecosystem-specific limitations. It aims to be entirely unsupervised, utilizing fewer and broader driver classes, and avoids thresholding or land cover masking, thereby enhancing its applicability across different regions. The changes that are here characterized are the largest detected changes with BFASTm-L2 in 20-year MODIS NDVI time series.

This section is divided into two sub-sections. The first discusses the results related to the change metrics proposed to better characterize the detected changes. The second focuses on the RGB map, proposed as an improved change map.

6.1. Contributing to the "How" facet: the magnitude, dissimilarity, and direction of change to improve change characterization

Detected changes are usually categorized as either abrupt or gradual changes depending on the duration of the change (Zhu et al., 2022). Sudden seasonal changes have not been explicitly addressed because: i) the detection of changes in dense SITS often requires the removal of the seasonality (Evans and Geerken, 2004; Hird et al., 2016), ii) they are mostly considered to be climate-driven changes (especially for erratic changes in amplitude), and iii) they typically result in small magnitudes of change (especially for LOS/NOS changes) (Ngadi Scarpetta et al., 2023). Because land use conversions, such as LSAI-driven ones in Senegal, typically involve seasonal changes that are not necessarily accompanied by abrupt changes, the effort in this study was to select metrics that effectively discriminate between types of changes.

The first change metric is the BFASTm-L2 magnitude of change, which is known to be sensitive to abrupt and large gradual changes, but also to NOS changes (Ngadi Scarpetta et al., 2023).Because many change drivers are likely to induce these types of changes, this map represented our baseline map, from which different drivers, all of which inducing high-intensity changes, were tentatively discriminated.

The second metric evaluated here was the dissimilarity metric introduced to help discriminate seasonal changes. This metric showed to be invariant to amplitude and trend changes, while being very sensitive to NOS/LOS changes and small intra-annual variability (Table 1 and Fig. 6). This metric was most effective in the Niayes, where it effectively highlighted LSAIs (Appendix C). In other regions, the dissimilarity shows a great sensitivity to the strong intra-annual variability present in the wetlands and estuaries, in the SR floodplain (Appendix B.d) and Casamance respectively. Although this metric shows a strong sensitivity to agricultural changes, it seems to be primarily sensitive to the seasonal changes caused by annual crops, rather than slow-growing plantations, as is the case with the arabica gum plantations in Ferlo (Appendix D).

Finally, the NDVI ratio based on the comparison of two 3-year periods after and before the change, provides an indication of the direction and intensity of the change. A 3-year period was considered sufficient to favor persistent changes over climate-driven changes. While this ratio improves the discrimination between biomass-producing and biomass-depleting drivers, we found that it was most useful for discriminating anthropogenic drivers such as mining or infrastructure (zooms 7–9,13 in Fig. 9), rather than LSAIs, which have highly variable NDVI ratios (Appendices B.e and C.e).

While each metric alone provides valuable insight into potential

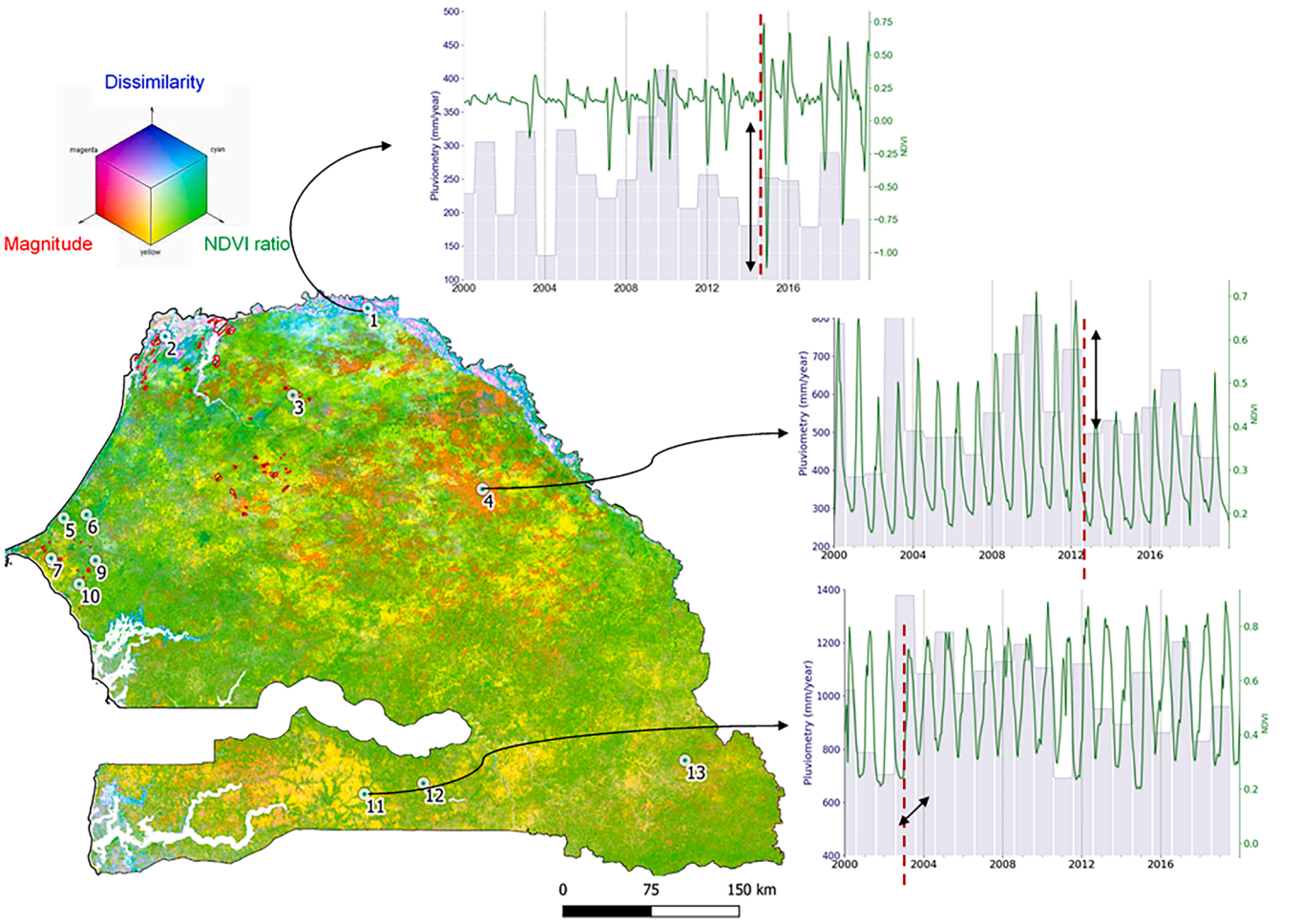

Fig. 8. RGB composite map with in Red: the change's magnitude, in Green: the NDVI ratio, and in Blue: the dissimilarity metric. MODIS 2000–2019 NDVI and TRMM annual rainfall distribution are shown for three pixels with natural/ climate-driven changes: 1 (wetland), 4 (shrub savanna) and 11 (dry tropical forest). See legend in Table 3. Map values were stretched between the 1st and 99th data percentiles, corresponding to [0.73–1.33] and [0–0.79] for NDVI ratio and dissimilarity, respectively. (For interpretation of the references to color in this figure legend, the reader is referred to the web version of this article.)

drivers of change, interpretation of these multiple changes independently is often complicated.

6.2. *Gaining insight into the 'Why' Facet of land change through the exploration of different change signatures displayed in an RGB Map*

6.2.1. *General considerations*

To date, most unsupervised studies have focused on disentangling climatic and anthropogenic drivers of LULC change based on the correlation between vegetation productivity and meteorological data (e.g. pluviometry) (Olsson et al., 2005), often using the Residual Trend Analysis (RESTREND, Evans and Geerken (2004)) (Anchang et al., 2019; Leroux et al., 2017). However, this approach relies heavily on the linear relationship between vegetation productivity and rainfall, making it applicable only under specific conditions (e.g., linear response of vegetation to increased precipitation, absence of severe land degradation).

In contrast, this study aims to identify drivers of change by leveraging the complementary nature of different change metrics that provide information about the type of change, its direction and intensity, integrated into an RGB change map, supported by visual spatial analysis at multiple scales. While shape parameters and change metrics are often included in supervised analyses that aim to identify specific drivers of change (Schroeder et al., 2017; Zhang et al., 2022), the relationship between major drivers of change and the types of changes involved has been less frequently studied.

In the current study, while the change detection is done at the pixel level, the attribution of possible drivers of change is done by looking at the color ("signature" of change), area, and shape of the clusters. The date of change map also helps in this process, as very large clusters of change with the same date of change are unlikely to have an anthropogenic origin. This is the case of the natural areas around points 4 and 11 in Fig. 8, which are most likely driven by pluviometry and natural forest regrowth respectively. These represent the most significant events occurring at any given time during the 2003–2018 monitoring period. While the current dynamics may be slightly different, this change map is powerful for detecting punctual human-induced events in the past, which tend to be more persistent over the time than other disturbance types. Compared to natural and climate-driven changes, anthropogenic land changes are spatially constrained, often with geometric shapes.

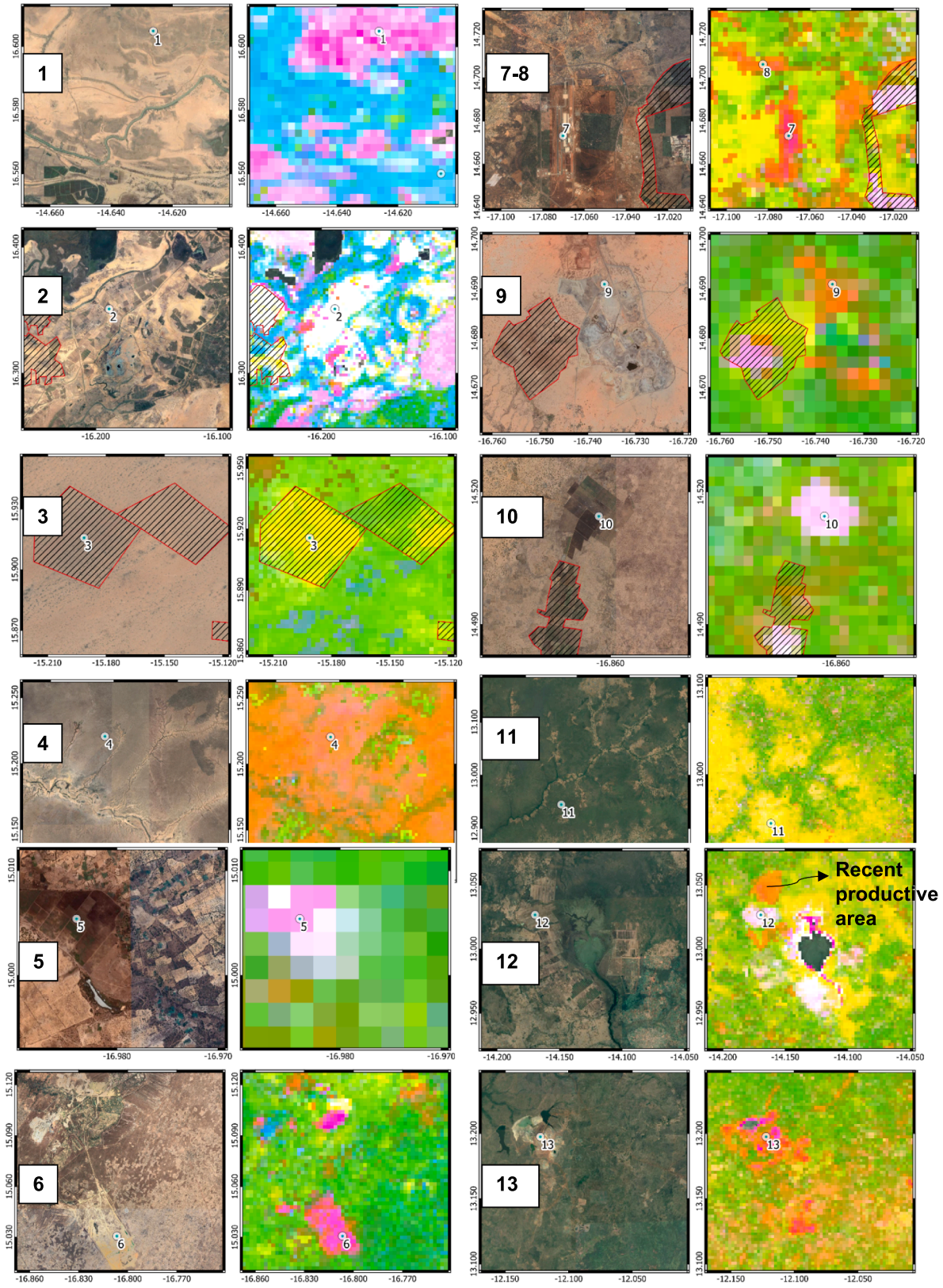

Fig. 9. Zoom-ins of study cases 1 to 13. LSAIs: 2, 3, 9, 10,12. Not in database LSAIs: points 5, 10. Mines: points 6 and 13. Infrastructures: points 7 (airport) and 8 (road). Forest: point 11. Wetland: point 1. Other natural vegetation: point 4.

6.2.2. LSAIs

While the LSAIs show different signatures of change across the country, most share high dissimilarities with different NDVI ratios, introducing a new way to characterize them. All LSAI-related changes appear in light pink/white, except for those in the Ferlo, which are yellow (very low dissimilarities). Specifically, LSAIs are best identified in the Niayes (Appendix C), where they are widely spaced and are coloured light pink (Figs. 9.5, 9.9, 9.10). In this region no other land dynamics produce the same signature of change. In the arid north (Appendix B), newly established LSAIs appear in white as a result of significant changes that represent land conversion from semi-arid natural vegetation to agribusiness. LSAIs established prior to the monitoring period and SR Valley wetlands characterized by flood recession agriculture both appear in light pink, making them difficult to distinguish. Finally, in the semitropical south, new LSAIs (or spatial extensions, i.e. the orange area in Fig. 9: Zoom-ins of study cases 1 to 13. LSAIs: 2, 3, 9, 10,12. Not in database LSAIs: points 5, 10. Mines: points 6 and 13. Infrastructures: points 7 (airport) and 8 (road). Forest: point 11. Wetland: point 1. Other natural vegetation: point 4..12) show negative abrupt changes that may be related to field preparation and biomass (woody vegetation) removal in favor of annual crops. In contrast to the north, plots of LSAIs installed before 2003 appear in very pale pink, indicating changes in agricultural practices. The presence of these white clusters near compact orange clusters may help distinguish LSAIs from other land dynamics in the tropics, even though in this region, as in the Niayes, no other land dynamics appear to produce the same colors.

Compared to other pixel-based studies aimed at detecting LSAI (Bey et al., 2020; Hentze et al., 2017; Hurni et al., 2017; Xiao et al., 2020), this approach has the advantage of being fast, unsupervised, not crop-specific, independent of absolute spectral values, and able to use all available data. Therefore, it can be used as the first step of a pipeline to detect potential LSAIs. Beyond Senegal, this approach has been validated in diverse geographical contexts, including Laos, Argentina, Mozambique, and Bolivia. Illustrations of the applications in Laos and Argentina are provided in Appendix B of the Ngadi Scarpetta (2024) thesis.

A more in-depth analysis could then be performed using High Resolution satellite imagery only at these specific locations, including morphological and textural metrics following Vogels et al. (2019). Because the detected changes represent the largest LULCC within the entire monitoring period, detected areas may have a different land use in the present.

6.3. Limitations and recommendations

Our results show that the RGB change-metric based map at the national scale proved to be useful for quick visual detection of specific land changes. However, there are some limitations. The first, as shown in Table 3, is that there is not a one-to-one relationship between a given combination of change types and a change agent. For example, while it is true that the reported Senegalese LSAIs are likely to cause seasonal NOS/LOS changes, other spatial objects such as the highly unstable estuaries and wetlands are also exhibit this type of change. In this case, other characteristics such as spatial patterns (area, shape) may help to determine the most likely driver of change. Similarly, the same type of change's agent can cause different combinations of change types. For example, certain types of LSAIs, such as those involving slow-growing tree plantations in semi-arid environments, do not cause visible NOS/LOS changes such as annual crops. These land dynamics are therefore poorly captured by BFASTm-L2. Finally, it is important to note that the results may be different in other climatic regions, especially in the humid tropics, where the observed seasonal changes may be less pronounced. The same conclusions apply to regions where the diversity and size of agricultural systems makes LSAI less contrasted with other agricultural land uses. Indeed, it is important to keep in mind that in Senegal, the majority of the farms are smallholdings, rain-fed, with an area of less than five hectares (Bourgoin et al., 2019).

Regarding some of the recommendations, it is worth noting that because the change magnitude is not NDVI normalized, for a same region encompassing different biomes (e.g. the Niayes), the magnitude tends to be higher over the forested areas. On the other hand, when considering the use of this method with other sensors, because BFASTm-L2 relies on long (at least 8 years) gap-free and smoothed time series, with a high temporal frequency to properly represent phenology, applications with higher resolution SITS such as Sentinel are currently hampered by the short temporal depth. The use of coarse resolution MODIS SITS allows rapid and easy identification of areas with specific land change dynamics over large areas, which can be analysed in more detail using High Resolution satellite imagery at a later stage.

7. Conclusions and perspectives

In this exploratory study, the BFASTm-L2 change detection algorithm was applied to MODIS 2000–2020 NDVI imagery to provide insights into the major land changes and potential drivers of change in Senegal, contributing in a novel way to the How and Why facets of land change proposed by Zhu et al. (2022). The How facet of land change was characterized here by three change metrics, namely the magnitude of change, the direction of change, and a time series shape dissimilarity metric. The combination of these metrics in an RGB composite map allowed the characterization of different land dynamics, and proved to be a useful visualization approach in detecting different anthropogenic LULCC such as those induced by LSAIs, mines or infrastructure. Complex land use systems such as LSAIs, which are diverse in terms of cropping practices, are often difficult to detect. However, by combining the "signature" of change, with other change characteristics such as the area and shape, newly installed (within the monitoring period) LSAIs could be visually inferred from the RGB map.

Although this approach has only been tested in Senegal, it demonstrates the usefulness of integrating the type of change, and in particular the seasonal ones, into the characterization of land change. This approach, based on a statistical change detection method, has the advantage of being interpretable, robust to noise and easily transferable to different regions, as it uses all the available temporal data and does not require the use of ancillary data. Further research will focus on automating the LSAI detection approach and integrating morphological and textural variables from high spatial resolution satellite imagery into the analysis. The approach will then be tested to different regions of the world.

CRediT authorship contribution statement

Yasmine Ngadi Scarpetta: Conceptualization, Data curation, Formal analysis, Investigation, Methodology, Software, Visualization, Writing – original draft. **Valentine Lebourgeois:** Funding acquisition, Project administration, Resources, Supervision, Writing – review & editing. **Mohamadou Dieye:** Data curation. **Anne-Elisabeth Laques:** Supervision, Writing – review & editing. **Agnès Begue:** Funding acquisition, Resources, Supervision, Writing – review & editing.

Declaration of competing interest

The authors declare the following financial interests/personal relationships which may be considered as potential competing interests: [Valentine Lebourgeois reports financial support was provided by French Space Agency. Yasmine Ngadi Scarpetta reports financial support was provided by French National Research Agency under the Investments for the Future program. Yasmine Ngadi Scarpetta reports financial support was provided by University of Montpellier. If there are other authors, they declare that they have no known competing financial interests or personal relationships that could have appeared to influence the work reported in this paper.].

Data availability

Data will be made available on request.

Acknowledgments

The authors thank the Land Matrix Initiative and the ISRA-BAME for data collection and support. This work was supported by the French Space Agency (CNES) (TOSCA-VISAGE project), and by the French National Research Agency under the Investments for the Future program #DigitAg (ANR-16-CONV-0004). Yasmine Ngadi received a scholarship from the University of Montpellier.

Author Contributions

Yasmine Ngadi processed the data, proposed and implemented the proposed methods, analyzed the results and wrote the paper; Mohamadou Dieye retrieved and processed the field database; Agnès Bégué, Valentine Lebourgeois and Anne-Elisabeth Laques supervised the research and contributed to the editing and review of the paper.

Appendix

Appendix A

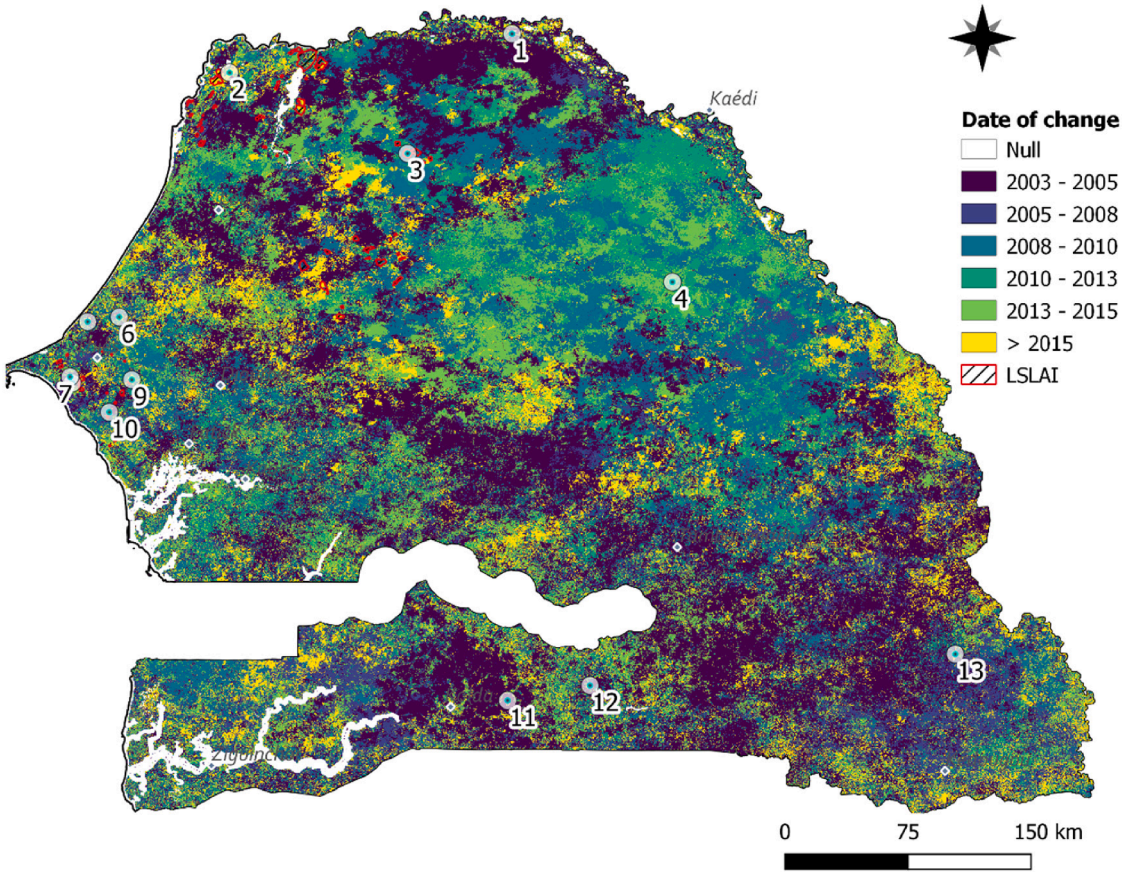

Date of change map

Date of change map.

Appendix B

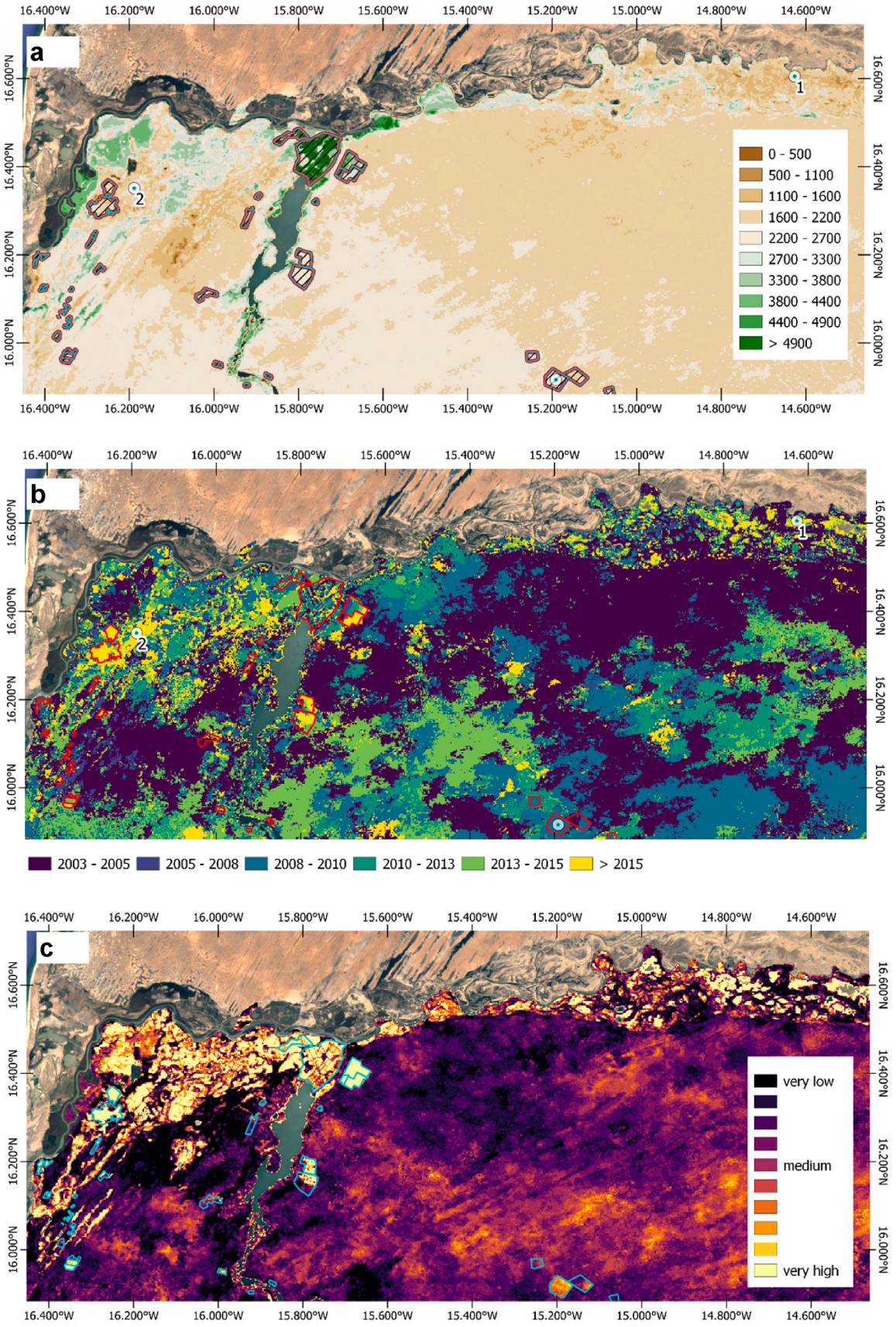
a
16.400°W
16.200°W
16.000°W
15.800°W
15.600°W
15.400°W
15.200°W
15.000°W
14.800°W
14.600°W
16.600°N
16.400°N
16.200°N
16.000°N
1
2
0 - 500
500 - 1100
1100 - 1600
1600 - 2200
2200 - 2700
2700 - 3300
3300 - 3800
3800 - 4400
4400 - 4900
> 4900
b
2003 - 2005
2005 - 2008
2008 - 2010
2010 - 2013
2013 - 2015
> 2015
c
very low
medium
very high

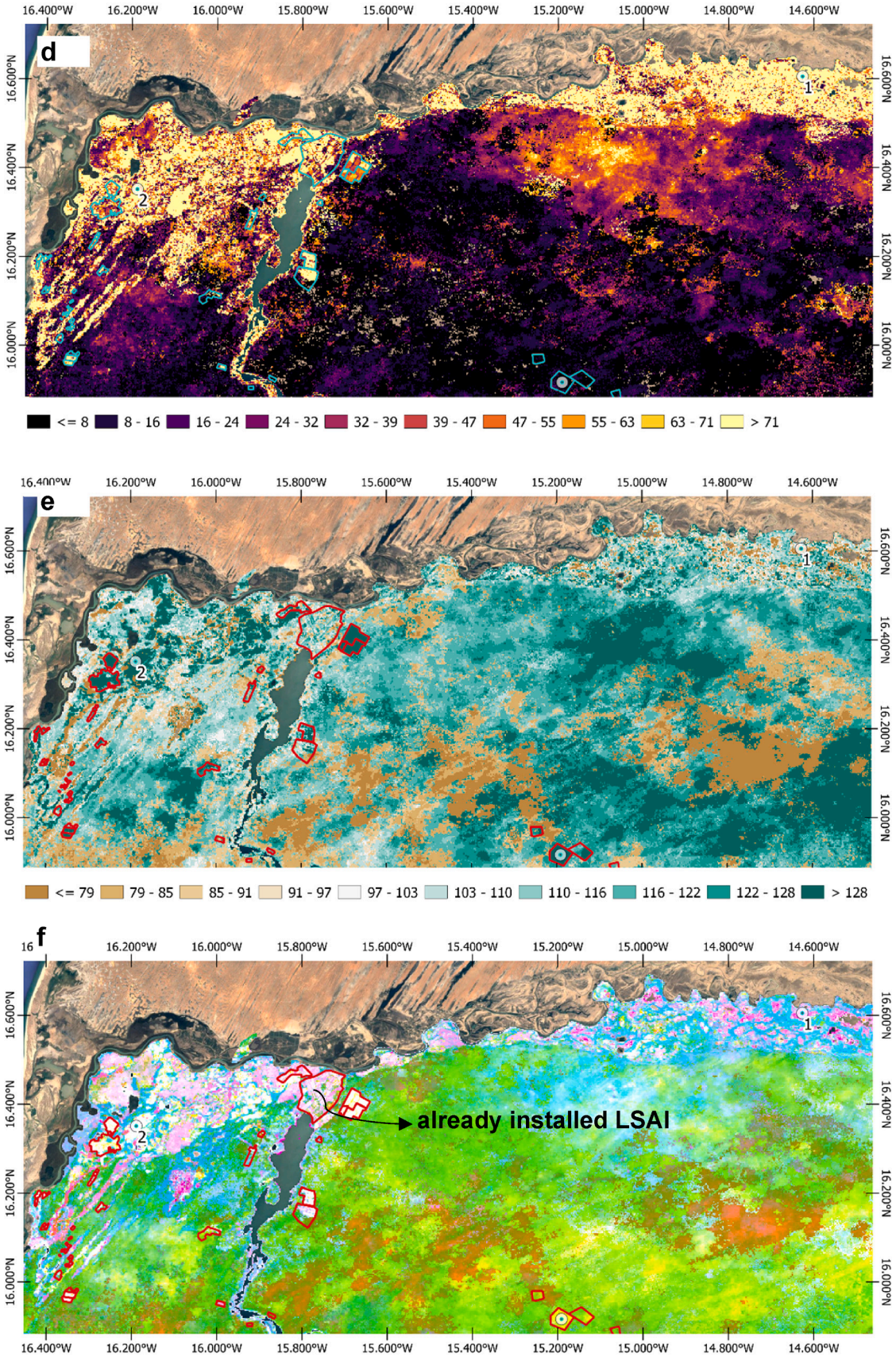

Close-in views of the Senegal River. a) MODIS NDVI 2000–2021 average map, b) Date of change map, c) Magnitude of change map, d) Dissimilairty map, e) NDVI ratio map, f) RGB map.

Appendix C

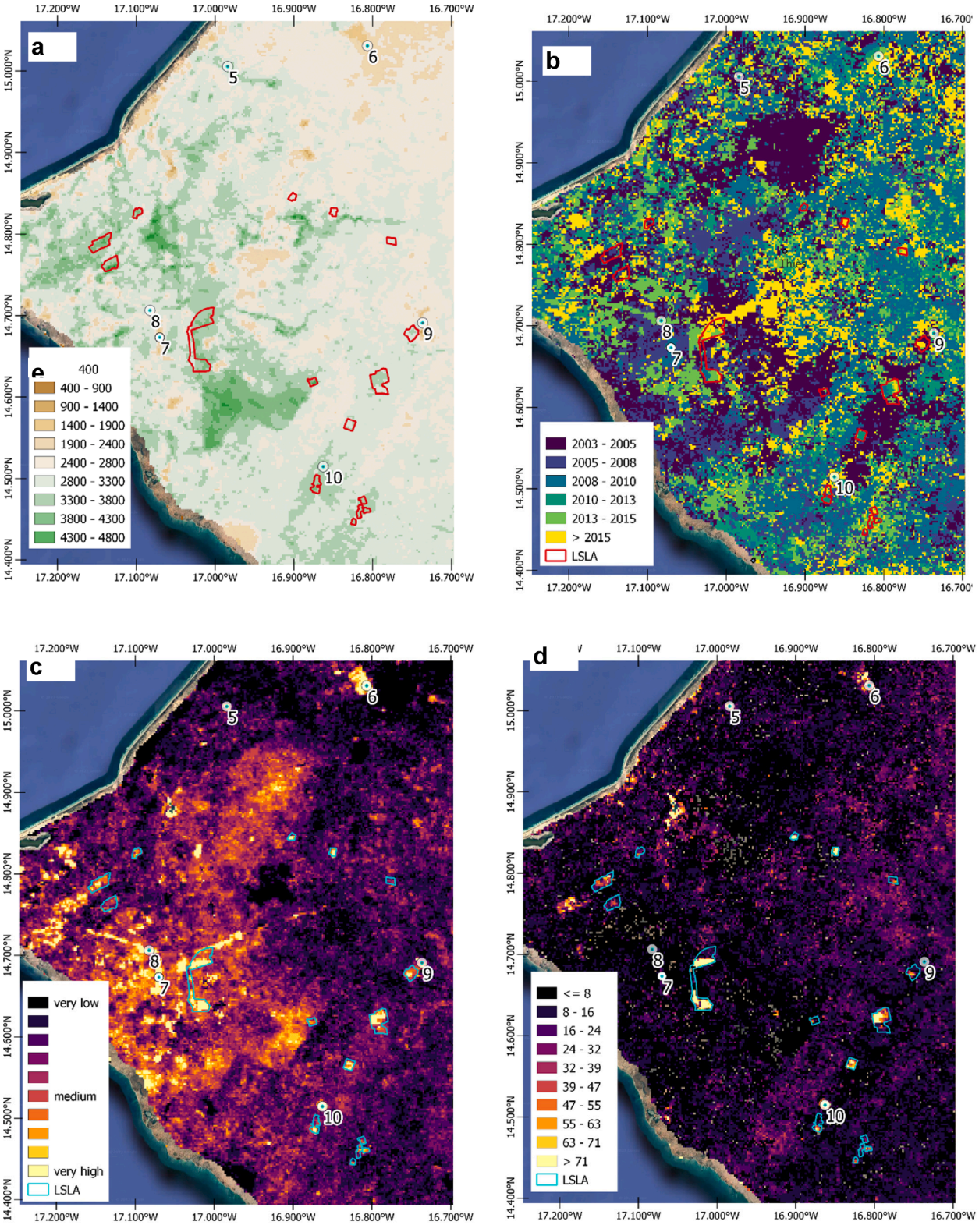
a
400
400 - 900
900 - 1400
1400 - 1900
1900 - 2400
2400 - 2800
2800 - 3300
3300 - 3800
3800 - 4300
4300 - 4800
b
2003 - 2005
2005 - 2008
2008 - 2010
2010 - 2013
2013 - 2015
> 2015
LSLA
c
very low
medium
very high
LSLA
d
<= 8
8 - 16
16 - 24
24 - 32
32 - 39
39 - 47
47 - 55
55 - 63
63 - 71
> 71
LSLA
17.200°W
17.100°W
17.000°W
16.900°W
16.800°W
16.700°W
15.000°N
14.900°N
14.800°N
14.700°N
14.600°N
14.500°N
14.400°N
5
6
7
8
9
10

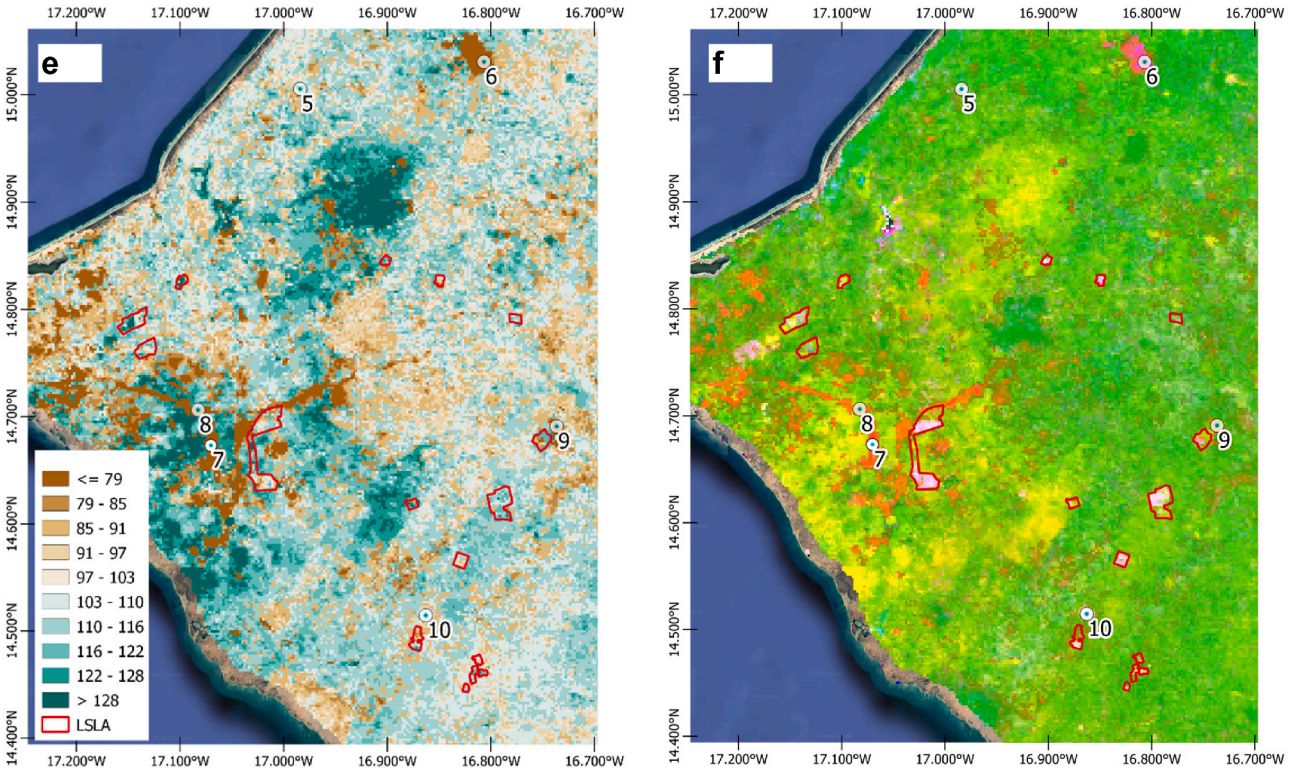

Close-in views of the Niayes. a) a) MODIS NDVI 2000–2021 average map, b) Date of change map, c) Magnitude of change map, d) Dissimilairty map, e) NDVI ratio map, f) RGB map.

Appendix D

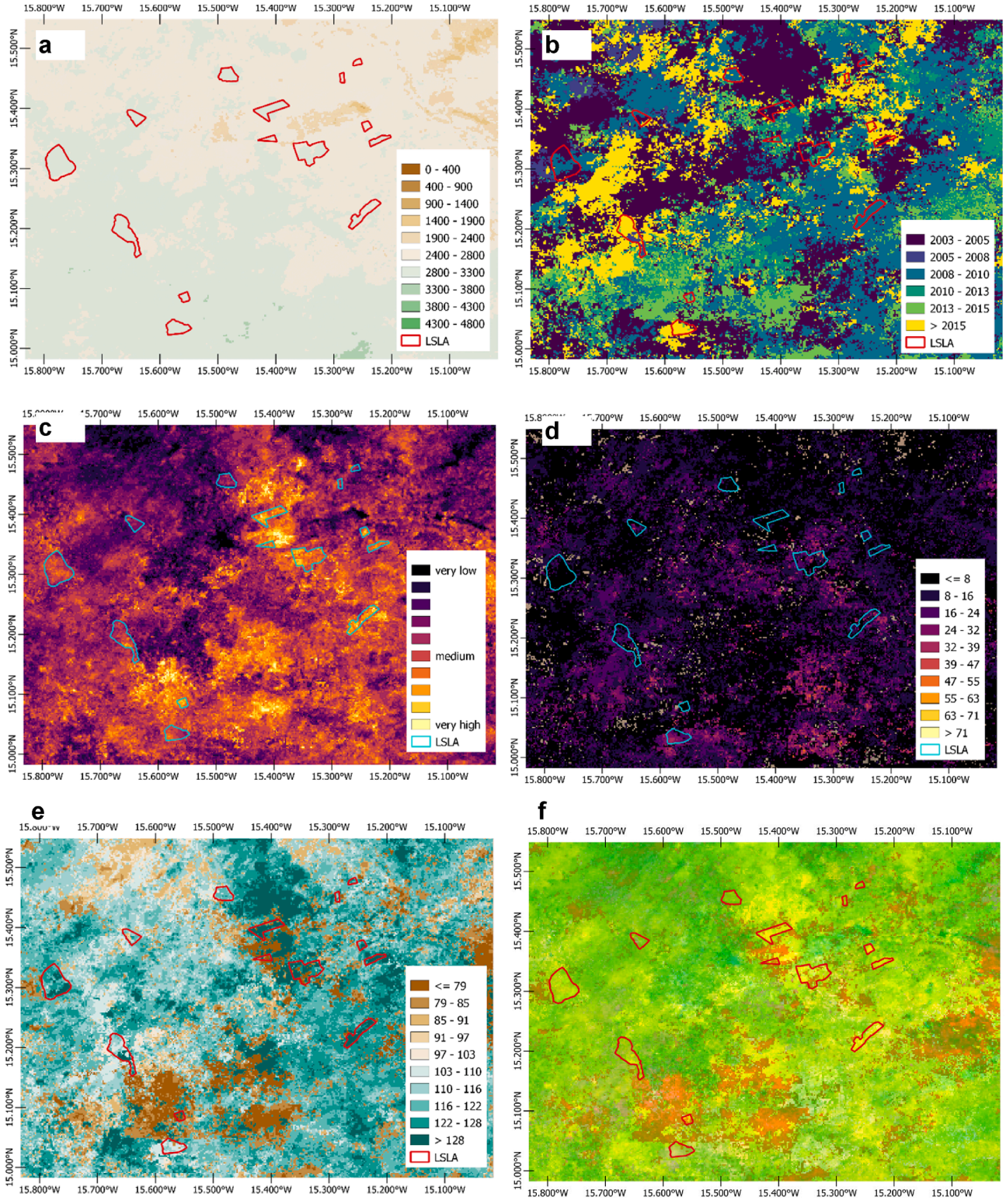

Close-in views of the Ferlo. a) MODIS NDVI 2000–2021 average map, b) Date of change map, c) Magnitude of change map, d) Dissimilairty map, e) NDVI ratio map, f) RGB map.

References

Anchang, J.Y., Prihodko, L., Kaptué, A.T., Ross, C.W., Ji, W., Kumar, S.S., Lind, B., Sarr, M.A., Diouf, A.A., Hanan, N.P., 2019. Trends in Woody and Herbaceous Vegetation in the Savannas of West Africa. Remote Sens. 11, 576. https://doi.org/10.3390/rs11050576.

Arvor, D., Meirelles, M., Dubreuil, V., Bégué, A., Shimabukuro, Y.E., 2012. Analyzing the agricultural transition in Mato Grosso, Brazil, using satellite-derived indices. Appl. Geogr. 32, 702–713. https://doi.org/10.1016/j.apgeog.2011.08.007.

Awty-Carroll, K., 2019. Simulated NDVI time series repository. Open Science Framework. https://doi.org/10.17605/OSF.IO/TAF9Y. https://osf.io/taf9y/.

Awty-Carroll, K., Bunting, P., Hardy, A., Bell, G., 2019. An Evaluation and Comparison of Four Dense Time Series Change Detection Methods Using Simulated Data. Remote Sens. 11, 2779. https://doi.org/10.3390/rs11232779.

Bey, A., Jetimane, J., Lisboa, S.N., Ribeiro, N., Sitoe, A., Meyfroidt, P., 2020. Mapping smallholder and large-scale cropland dynamics with a flexible classification system and pixel-based composites in an emerging frontier of Mozambique. Remote Sens. Environ. 239, 111611 https://doi.org/10.1016/j.rse.2019.111611.

Bourgoin, J., Valette, E., Guillouet, S., Diop, D., Dia, D., 2019. Improving Transparency and Reliability of Tenure Information for Improved Land Governance in Senegal. Land 8, 42. https://doi.org/10.3390/land8030042.

Brown, J.C., Jepson, W.E., Kastens, J.H., Wardlow, B.D., Lomas, J.M., Price, K.P., 2007. Multitemporal, Moderate-Spatial-Resolution Remote Sensing of Modern Agricultural Production and Land Modification in the Brazilian Amazon. GIScience remote sens 44, 117–148. https://doi.org/10.2747/1548-1603.44.2.117.

Browning, D.M., Maynard, J.J., Karl, J.W., Peters, D.C., 2017. Breaks in MODIS time series portend vegetation change: verification using long-term data in an arid grassland ecosystem. Ecological Applications : a Publication of the Ecological Society of America 27, 1677–1693. https://doi.org/10.1002/eap.1561.

Budde, M., Tappan, G., Rowland, J., Lewis, J., Tieszen, L., 2004. Assessing land cover performance in Senegal, West Africa using 1-km integrated NDVI and local variance analysis. J. Arid Environ. 59, 481–498. https://doi.org/10.1016/j.jaridenv.2004.03.020.

Chen, J., Jönsson, P., Tamura, M., Gu, Z., Matsushita, B., Eklundh, L., 2004. A simple method for reconstructing a high-quality NDVI time-series data set based on the Savitzky-Golay filter. Remote Sens. Environ. 91, 332–344. https://doi.org/10.1016/j.rse.2004.03.014.

Chen, S., Olofsson, P., Saphangthong, T., Woodcock, C.E., 2023. Monitoring shifting cultivation in Laos with Landsat time series. Remote Sens. Environ. 288, 113507 https://doi.org/10.1016/j.rse.2023.113507.

Evans, J., Geerken, R., 2004. Discrimination between climate and human-induced dryland degradation. J. Arid Environ. 57, 535–554. https://doi.org/10.1016/S0140-1963(03)00121-6.

Geerken, R.A., 2009. An algorithm to classify and monitor seasonal variations in vegetation phenologies and their inter-annual change. ISPRS J. Photogramm. Remote Sens. 64, 422–431. https://doi.org/10.1016/j.isprsjprs.2009.03.001.

Gower, J.C., 1975. Generalized procrustes analysis. Psychometrika 40, 33–51.

Harding, A., Chamberlain, W., Anseeuw, W., Manco, G., Niassy, S., 2016. Large-scale land acquisitions profile. Senegal, Land Matrix https://landmatrix.org/documents/60/LM_Country_Profile_Senegal_English.pdf (accessed 1 June 2023.

Hentze, K., Thonfeld, F., Menz, G., 2017. Beyond trend analysis: How a modified breakpoint analysis enhances knowledge of agricultural production after Zimbabwe's fast track land reform. Int. J. Appl. Earth Obs. Geoinf. 62, 78–87. https://doi.org/10.1016/j.jag.2017.05.007.

Hird, J.N., Castilla, G., McDermid, G.J., Bueno, I.T., 2016. A Simple Transformation for Visualizing Non-seasonal Landscape Change From Dense Time Series of Satellite Data. IEEE J. Sel. Top. Appl. Earth Observations Remote Sensing 9, 3372–3383. https://doi.org/10.1109/JSTARS.2015.2419594.

Horowitz, M.M., Salem-Murdock, M., 1993. Development-induced food insecurity in the middle Senegal Valley. GeoJournal 30, 179–184. https://doi.org/10.1007/BF00808136.

Hurni, K., Schneider, A., Heinimann, A., Nong, D., Fox, J., 2017. Mapping the Expansion of Boom Crops in Mainland Southeast Asia Using Dense Time Stacks of Landsat Data. Remote Sens. 9, 320. https://doi.org/10.3390/rs9040320.

Julien, Y., Sobrino, J.A., 2021. Introducing the Time Series Change Visualization and Interpretation (TSCVI) method for the interpretation of global NDVI changes. Int. J. Appl. Earth Obs. Geoinf. 96, 102268 https://doi.org/10.1016/j.jag.2020.102268.

Kennedy, R.E., Yang, Z., Braaten, J., Copass, C., Antonova, N., Jordan, C., Nelson, P., 2015. Attribution of disturbance change agent from Landsat time-series in support of habitat monitoring in the Puget Sound region, USA. Remote Sens. Environ. 166, 271–285. https://doi.org/10.1016/j.rse.2015.05.005.

Kummerow, C., Barnes, W., Kozu, T., Shiue, J., Simpson, J., 1998. The Tropical Rainfall Measuring Mission (TRMM) Sensor Package. J. Atmos. Oceanic Technol. 15, 809–817. https://doi.org/10.1175/1520-0426(1998)015<0809:TTRMMT>2.0.CO;2.

Leroux, L., Bégué, A., Lo Seen, D., Jolivot, A., Kayitakire, F., 2017. Driving forces of recent vegetation changes in the Sahel: Lessons learned from regional and local level analyses. Remote Sens. Environ. 191, 38–54. https://doi.org/10.1016/j.rse.2017.01.014.

Lhermitte, S., Verbesselt, J., Verstraeten, W.W., Coppin, P., 2011. A comparison of time series similarity measures for classification and change detection of ecosystem dynamics. Remote Sens. Environ. 115, 3129–3152. https://doi.org/10.1016/j.rse.2011.06.020.

Mardian, J., Berg, A., Daneshfar, B., 2021. Evaluating the temporal accuracy of grassland to cropland change detection using multitemporal image analysis. Remote Sens. Environ. 255, 112292 https://doi.org/10.1016/j.rse.2021.112292.

Masiliūnas, D., Tsendbazar, N.-E., Herold, M., Verbesselt, J., 2021. BFAST Lite: A Lightweight Break Detection Method for Time Series Analysis. Remote Sens. 13, 3308. https://doi.org/10.3390/rs13163308.

Molinier, M., Miettinen, J., Ienco, D., Qiu, S., Zhu, Z., 2021. Optical satellite image time series analysis for environment applications: From classical methods to deep learning and beyond. In: Change Detection and Image Time Series Analysis 2: Supervised Methods, pp. 109–154.

Ngadi Scarpetta, Y., Lebourgeois, V., Laques, A.-E., Dieye, M., Bourgoin, J., Bégué, A., 2023. BFASTm-L2, an unsupervised LULCC detection based on seasonal change detection – An application to large-scale land acquisitions in Senegal. Int. J. Appl. Earth Observ. Geoinform. 121, 103379 https://doi.org/10.1016/j.jag.2023.103379.

Ngadi Scarpetta, Y., 2024. From Land Cover to Land Use Systems Mapping: Detection and Characterization of Large Scale Agricultural Investments (LSAIs) from Satellite Imagery. Application to Senegal. [Doctoral dissertation, Université de Montpellier]. Montpellier.

Nolte, K., Chamberlain, W., Giger, M., 2016. International Land Deals for Agriculture: fresh insights from the Land Matrix: Analytical Report II. Bern Open Publ, Bern, pp. 68–pp.

Olsson, L., Eklundh, L., Ardö, J., 2005. A recent greening of the Sahel—trends, patterns and potential causes. J. Arid Environ. 63, 556–566. https://doi.org/10.1016/j.jaridenv.2005.03.008.

Piou, C., Lebourgeois, V., Benahi, A.S., Bonnal, V., Jaavar, M.e.H., Lecoq, M., Vassal, J.-M., 2013. Coupling historical prospection data and a remotely-sensed vegetation index for the preventative control of Desert locusts. Basic Appl. Ecol. 14, 593–604. https://doi.org/10.1016/j.baae.2013.08.007.

Radwan, T.M., Blackburn, G.A., Whyatt, J.D., Atkinson, P.M., 2021. Global land cover trajectories and transitions. Sci. Rep. 11, 12814. https://doi.org/10.1038/s41598-021-92256-2.

Rodríguez Paulino, E., Schlerf, M., Röder, A., Stoffels, J., Udelhoven, T., 2024. Forest disturbance characterization in the era of earth observation big data: A mapping review. Int. J. Appl. Earth Obs. Geoinf. 128, 103755 https://doi.org/10.1016/j.jag.2024.103755.

Schroeder, T.A., Schleeweis, K.G., Moisen, G.G., Toney, C., Cohen, W.B., Freeman, E.A., Yang, Z., Huang, C., 2017. Testing a Landsat-based approach for mapping disturbance causality in U.S. forests. Remote Sens. Environ. 195, 230–243. https://doi.org/10.1016/j.rse.2017.03.033.

Setiawan, Y., Yoshino, K., 2012. Change detection in land-use and land-cover dynamics at a regional scale from MODIS time-series imagery. ISPRS Ann. Photogramm. Remote Sens. Spatial. Inf. Sci. I-7, 243–248. https://doi.org/10.5194/isprsannals-I-7-243-2012.

Solly, B., Charahabil, M., Dieye, E., Sy, O., Barry, B., Sagna, B., Faye, C., 2020. Impacts of natural and anthropogenic factor on the woody flora of Haute-Casamance (South Senegal): from perception to reality. J. Appl. Sci. Envir. Stud. 3, 117–131.

Sultan, B., Janicot, S., 2003. The West African Monsoon Dynamics. Part II: The "Preonset" and "Onset" of the Summer Monsoon. J. Climate 16, 3407–3427. https://doi.org/10.1175/1520-0442(2003)016<3407:TWAMDP>2.0.CO;2.

Tappan, G., Sall, M., Wood, E., Cushing, M., 2004. Ecoregions and land cover trends in Senegal. J. Arid Environ. 59, 427–462. https://doi.org/10.1016/j.jaridenv.2004.03.018.

United Nations Office for the Coordination of Humanitarian Affairs. Sahel Crisis: 2011-2017. https://reliefweb.int/disaster/ot-2011-000205-ner (accessed 17 July 2023).

Verbesselt, J., Zeileis, A., Herold, M., 2012. Near real-time disturbance detection using satellite image time series. Remote Sens. Environ. 123, 98–108. https://doi.org/10.1016/j.rse.2012.02.022.

Verburg, P.H., van de Steeg, J., Veldkamp, A., Willemen, L., 2009. From land cover change to land function dynamics: a major challenge to improve land characterization. J. Environ. Manage. 90, 1327–1335. https://doi.org/10.1016/j.jenvman.2008.08.005.

Vogels, M., de Jong, S.M., Sterk, G., Addink, E.A., 2019. Mapping irrigated agriculture in complex landscapes using SPOT6 imagery and object-based image analysis – A case study in the Central Rift Valley, Ethiopia –. Int. J. Appl. Earth Obs. Geoinf. 75, 118–129. https://doi.org/10.1016/j.jag.2018.07.019.

Weiss, M., Jacob, F., Duveiller, G., 2020. Remote sensing for agricultural applications: A meta-review. Remote Sens. Environ. 236, 111402. https://doi.org/10.1016/j.rse.2019.111402.

Winkler, K., Fuchs, R., Rounsevell, M., Herold, M., 2021. Global land use changes are four times greater than previously estimated. Nat. Commun. 12, 2501. https://doi.org/10.1038/s41467-021-22702-2.

Woodcock, C.E., Loveland, T.R., Herold, M., Bauer, M.E., 2020. Transitioning from change detection to monitoring with remote sensing: A paradigm shift. Remote Sens. Environ. 238, 111558 https://doi.org/10.1016/j.rse.2019.111558.

Xiao, C., Li, P., Feng, Z., Liu, Y., Zhang, X., 2020. Sentinel-2 red-edge spectral indices (RESI) suitability for mapping rubber boom in Luang Namtha Province, northern Lao PDR. Int. J. Appl. Earth Obs. Geoinf. 93, 102176 https://doi.org/10.1016/j.jag.2020.102176.

Zhang, Y., Woodcock, C.E., Chen, S., Wang, J.A., Sulla-Menashe, D., Zuo, Z., Olofsson, P., Wang, Y., Friedl, M.A., 2022. Mapping causal agents of disturbance in boreal and arctic ecosystems of North America using time series of Landsat data. Remote Sens. Environ. 272, 112935 https://doi.org/10.1016/j.rse.2022.112935.

Zhao, K., Wulder, M.A., Hu, T., Bright, R., Wu, Q., Qin, H., Li, Y., Toman, E., Mallick, B., Zhang, X., Brown, M., 2019. Detecting change-point, trend, and seasonality in satellite time series data to track abrupt changes and nonlinear dynamics: A Bayesian ensemble algorithm. Remote Sens. Environ. 232, 111181 https://doi.org/10.1016/j.rse.2019.04.034.

Zhu, Z., Qiu, S., Ye, S., 2022. Remote sensing of land change: A multifaceted perspective. Remote Sens. Environ. 282, 113266 https://doi.org/10.1016/j.rse.2022.113266.